AD-A138 379 ON THE STABILITY OF FLIGHT VEHICLES IN THE LOW REYNOLDS 1/1
NUMBE NON-LINEAR..(U) MASSACHUSETTS INST OF TECH
CAMBRIDGE DEPT OF AERONAUTICS AND A..
UNCLASSIFIED E E COVERT ET AL. JAN 84 N00014-82-K-0310 F/G 20/4 NL

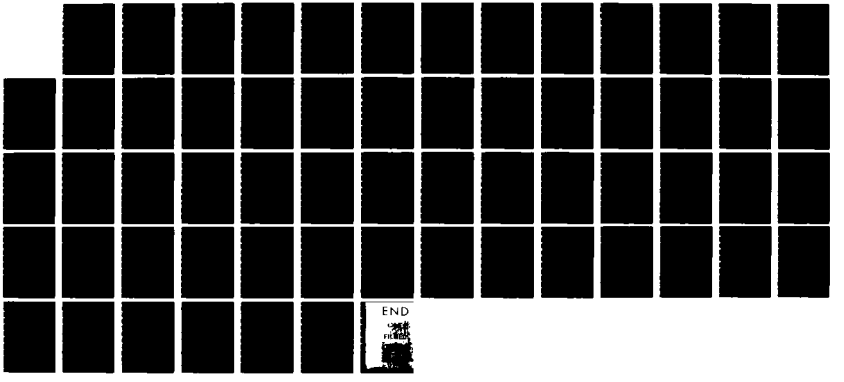

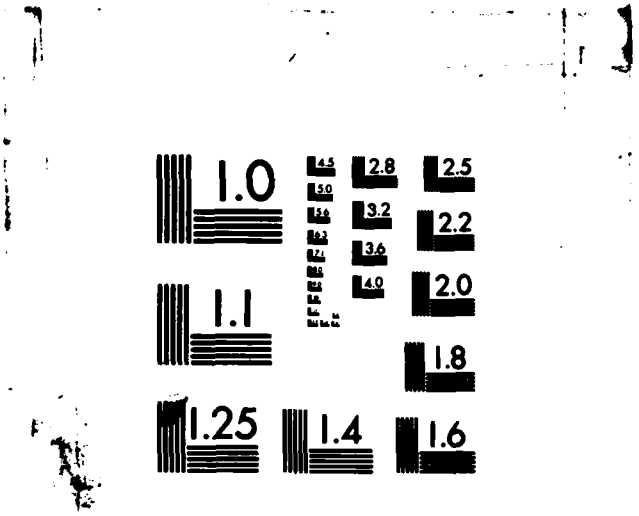

MICROCOPY RESOLUTION TEST CHART
NATIONAL BUREAU OF STANDARDS-1963-A

(12)

GAS TURBINE AND PLASMA DYNAMICS LABORATORY
DEPARTMENT OF AERONAUTICS AND ASTRONAUTICS
MASSACHUSETTS INSTITUTE OF TECHNOLOGY
CAMBRIDGE, MA 02139

AN INTERIM REPORT

on

ONR CONTRACT NO: N00014-82-K-0310

entitled

ON THE STABILITY OF FLIGHT VEHICLES IN THE LOW REYNOLDS NUMBER NON-LINEAR REGIME

prepared for

Department of the Navy
Office of Naval Research, Code 432F
800 North Quincy Street
Arlington, VA 22217
Attn: Dr. Robert Whitehead
Head, Fluid Mechanics Division

AUTHORS:

E. E. Covert
Director, Gas Turbine & Plasma Dynamics Lab
Professor of Aeronautics & Astronautics

Otto W. K. Lee
Graduate Research Assistant
Department of Aeronautics & Astronautics

Carol M. Vaczy
Graduate Research Assistant
Department of Aeronautics & Astronautics

January 1984

ACKNOWLEDGEMENT

This work was performed under the auspices of ONR Contract No. N00014-82-K-0310, under the direction of Dr. Robert Whitehead, Technical Monitor.

Letter on file

A-1

ON THE STABILITY OF FLIGHT VEHICLES IN THE LOW REYNOLDS NUMBER NON-LINEAR REGIME

by

Otto W. K. Lee

Carol M. Vaczy

Eugene E. Covert

Introduction

This report addresses some issues associated with dynamic stability of vehicles flying at speeds such that the flight Reynolds number is of the order of a few hundreds of thousands. In particular the wing loading and speed are such that the flight occurs at relatively high angles of attack. Under these circumstances the aerodynamic characteristics of the vehicle are likely to be non-linear in nature. Here the nature of the flight itself could be significantly different from that expected under those conditions where the aerodynamic characteristics are linear. Under those conditions the ideas underlying stability are fairly well understood. The issues are discussed clearly in several books that are readily available to anyone interested in learning more about the topic. Two that come to mind at once are Etkin's Airplane Dynamic Stability, and Control[1] and McCormack's, Aerodynamics, Aeronautics and Flight Mechanics[2]. There are other excellent books and their omission is not to be interpreted as a denigration. It is simply that the authors are most familiar with those two. Both these books have a fairly complete history of the study of dynamic stabiity of flying machines, starting with E.B. Wilson in the

United States, and Bryan in Great Britain. The subject was well understood by the late 20's and early 30's as the reader may decide by reading B.M. Jones's article in Volume V of Durand's Aerodynamic Theory[3]. The basic problems of the coupling of the aerodynamic characteristics to the motion is discussed there for a variety of special cases that lead to understanding of the complete problem. The modern reader may find the presentation itself difficult to follow because the current notation is clearer, and because the examples are somewhat archaic.

Indeed many improvements have been made in the matter of computing the values of the aerodynamic derivatives themselves, as well as in the matter of displaying the stability itself. In the present case a similar problem exists, even in comparison with the References 1 and 2. There are two reasons for this problem. First, in the low Reynolds number regime, a number of non-linearities appear in the aerodynamic characteristics which preclude, at least initially, the use of the so-called stability derivatives. Second, the separation into the symmetric and antisymmetric motion may not be realistic. Finally, there is the matter of determining the aerodynamic characteristics themselves in the low Reynolds number regime. In the discussion that follows, each of these issues will be treated. The method of approaching these issues will follow the currently accepted spirit of mathematical modeling. That is, the goal is to retain the primary physical processes in a convenient form that allows the results to be representative of those that could be obtained if a truer representation of the physical

phenomena either were available. An example of the latter might be to couple the rigid body motion to the Navier-Stokes equations, and to a representation of the vehicle's configuration. In principle this would allow for a complete solution of the motion along a flight path. In practice, it is not clear that such a step would be possible, let alone practical. And even if it were, the issue of determining the stability in a practical form for discussion would still have to be faced. In this discussion an approximate way of estimating the aerodynamic characteristic will be discussed first. The issue of stability and its representation will be discussed.

Equations of Motion

The equations of motion will be written in a standard form. The origin of the coordinate system is located at the center of mass of the vehicle and is assumed to be fixed. The x-axis points forward. The y-axis is to the right if one is looking in the positive x direction. The z-axis completes the orthogonal set, and is therefore positive downward from the x-y plane. The components of linear velocity along the x,y,z axes are u,v,w respectively. Corresponding to the linear velocity vector, the components of the angular velocity vector are p,q,r along the x,y,z axes. The components of angular momentum can be written as $H_i = I_{ij}\, p_i$. In this shorthand the summation notation is used and p_1 corresponds to p, p_2 = q, and p_3 = r. Note the usual assumption of lateral symmetry has been made so the products of inertia

$I_{12} = I_{xy} = 0$ and

$$I_{23} = I_{yz} = 0.$$

The product of inertia in the pitch plane

$$I_{13} = I_{xz}$$

is normally small, and in this case it seems to be slightly negative. Thus, the yawing angular velocity reduces the angular momentum in roll, and conversely. Ultimately this effect was neglected due to a lack of information about the inner disposition of dense equipment inside the vehicle. We chose to write the dynamical equations in first order form as shown below:

$$\frac{d}{dt}\begin{bmatrix} u \\ v \\ w \\ p \\ q \\ r \end{bmatrix} = -\begin{bmatrix} o & -r & q \\ r & o & p \\ -q & p & o \\ o & r & q \\ r & o & p \\ -q & p & o \end{bmatrix} \cdot \begin{bmatrix} u \\ v \\ w \\ p \\ q \\ r \end{bmatrix} + \begin{bmatrix} F_x/m - g \sin\theta \\ F_x/m + g \cos\theta \sin\phi \\ F_y/m + g \cos\theta \cos\phi \\ M_x/I_{xx} \\ M_y/I_{yy} \\ M_z/I_{zz} \end{bmatrix}$$

This set of equations needs to be related to a space fixed set if altitude and distance are important variables. This relation is accomplished by defining a rotation matrix that puts the velocity vector (u,v,w) into and earth fixed system (U,V,W). Then one integrates the resulting equation to give the position vector (X,Y,Z). Conceptually, and computationally, the easiest way to carry derive this set is to compute the rate change of the direction cosines of the X,Y,Z set in the x,y,z frame. Physically the Euler angles are easier to visualize, and thus this form was used, namely

$$\dot{\phi} = p + q \sec\theta \tan\theta \sin\phi + r \tan\theta \cos\phi$$

$$\dot{\theta} = q \cos\phi - r \sin\phi$$

$$\dot{\psi} = -q \sin\phi + r \sec\theta \cos\phi$$

and the R matrix used for the transformation

$$\begin{bmatrix} U \\ V \\ W \end{bmatrix} = \begin{bmatrix} R \end{bmatrix} \cdot \begin{bmatrix} u \\ v \\ w \end{bmatrix}$$

and,

$$[R] = \begin{bmatrix} \cos\psi\cos\theta & -\sin\psi\cos\phi + \cos\psi\sin\theta\sin\phi & \sin\psi\sin\phi + \cos\psi\sin\theta\cos\phi \\ \sin\psi\cos\theta & \cos\psi\cos\phi + \sin\psi\sin\theta\sin\phi & -\sin\psi\sin\phi + \cos\psi\sin\theta\cos\phi \\ -\sin\theta & \cos\theta\sin\phi & \cos\theta\cos\phi \end{bmatrix}$$

Note here the order of the rotation is to yaw nose to the right about the body fixed z-axis (or the earth fixed Z-axis since they are colinear at this point) to the angle ψ. Then one pitches nose up about the body fixed y-axis to the angle θ and finally rolls about the body fixed x-axis to the angle ϕ. Note the calculation of the Euler angles involves knowing the angular velocities about the vehicle body axis.

Any integration of these equations requires initial conditions. For our purposes we have selected equilibrium conditions followed by an upset in the velocity conditions. We have based the equilibirum state upon the aerodynamic characteristics measured in the wind tunnel[7].

Aerodynamic Characteristics

The calculation of the aerodynamic characteristics of the vehicle may be determined at several levels of sophistication. For the purposes of this study it is sufficient to assume that the two-dimensional airfoil characteristics, i.e., the section lift, drag, and moment coefficients, are available as functions of the angle of attack, at the

flight Reynolds number. It will be assumed that this section data is applicable to the flight circumstances. That is, it will be assumed the effects of vibration on the aerodynamic coefficients, either in the wind tunnel or in flight, are the same. It will be further assumed that the surface conditions are similar too. These assumptions are made primarily in the hope that the stability phenomena will be the same. One further assumption is necessary. That is the assumption of quasi-steady flow. Undoubtedly this assumption may not be valid, but lacking data, or realistic computations, it is necessary to make this assumption.

The simplest approach to the calculation of the aerodynamic characteristics is to use "strip theory." In this approximation the local sidewash, upwash, and longitudinal velocity components are used to determine the local flow angles and the local dynamic pressure. This allows one to determine the local section characteristics of the wing and the tail. By the appropriate integration one can determine the instantaneous forces and moments. In so far as the local velocities include the effects of the angular motion as well as the linear motion, the forces and moments reflect those effects. Indeed, if the rolling motion induces a stall, the change in the pitch plane forces and moments appears in a natural way. There are two serious objections to the use of strip theory. The loading is not diminished at the tip due to the shed vorticity, and hence the tip effects are weighted excessively. This is clearly shown by examination of the results summarized by Betz[4]. The other serious objection is due to

the implicit assumption that the flow remains more or less in the relative free stream direction. Winkleman's surface flow pictures[5] clearly show that this implicit assumption is wrong. However, until better means are available to correct for this lack of tools, one must hope the net results will not be too greatly in error.

The limitations of strip theory can be at least partially alleviated through the use of Prandtl's integral equation. This equation allows one to write the distribution of downwash due to the non-uniform circulation distribution through an integral of the spanwise drivative of the circulation. This derivative is closely related to the shed vorticity, which induces the downwash. The local angle of attack can be computed, including the downwash, and the section characteristics determined. The result is a functional integral equation that can be solved by iteration. The solution of this problem is fairly complicated since the principal part of the integral is needed. One can expand the integrand in a Fourier Series, and use Glauert's integral formula to obtain a complicated functional equation. Fortunately an approximation due to Schrenk[5] is usually accurate, and much simpler to use. This approximation is based upon a three-step process. First, one calculates the strip theory loading, and integrates it to obtain, say, the lift coefficient. Then, one finds the quarter or half ellipse that has the same area under it as the strip theory integral, which is really an algebraic step. The estimate of the actual span-wise loading is then the average of the strip theory and the ellipse. In the case of a rolling or yawing wing the elliptical distribution is multiplied by a

correction term of the form (1 + k times 2y/b) to give the estimate of asymmetric effects on the loading. The value of "k" can be estimated using the fundamental integral equation, and linear aerodynamics. The analysis describing this use of Schrenk's approximation will be given below.

Increasing sophistication would require, effectively, a correction to the camber of the airfoil due to the effects of the flow field due to the adjacent sections. In view of the fact that the initial correction due to the downwash is only handled approximately, it seems unreasonable to even attempt to apply the higher order correction.

Application of Schrenk's Approximation

The calculation that was discussed above really involves two steps. The first step is the determination of the local geometric angle of attack. This follows from the determination of the local linear and angular velocities. in the case of the horizontal tail one must account for the downwash due to the forward wing, as well. After the local angle of attack is known, one can follow Schrenk's procedure for all the symmetric cases. The procedure must be modified in application to the asymmetric motions due to rolling and yawing. In this case an extra term, which contributes zero net force, is proportional to

$$(2y/b)\sqrt{1 - (2y/b)2}$$

or sine two theta where theta is arccosine (2y/b). The constant of proportionality is found such that the area under the strip theory loading on one halfspan curve has the same value as that described by

the terms above. In the particular geometry used here, a result that was essentially equal to that obtained by the Schrenk procedure could be found by simply using strip theory to calculate the lift, say, and then comparing that estimate with the measured lift from the wind tunnel in ratio form. The resulting ratio was then applied to all strip theory results. This step reduced the amount of calculation considerably. The loss in accuracy was such that the damping terms due to angular motion were too small, so the procedure was felt to be conservative.

Analyis of Stability

The analysis of stability will follow three specific steps. First, the stability derivatives given in Ref. 7 will be used in a classical stability analysis following the procedures outlined by Etkin[1]. The elementary pitch plane analysis will be applied to the pitch plane only that is based upon the local value of the aerodynamic loads. Finally, an analysis of the full non-linear equations will be presented. This analysis will be based upon the ideas of Liapunov[8]. Liapunov stability is based upon the concept of the phase plane. The phase plane is a plane whose coordinates are the velocity and the displacement. The dynamic motion is represented as a locus, or trajectory, in the phase plane. Each point on the trajectory corresponds to the instantaneous state, that is, the instantaneous velocity and position. An equilibrium position is a point on this plane, if the equilibrium is a steady state. If the equilibrium corresponds to a limit cycle then the trajectory in the phase plane is a closed curve. Naturally if the motion traces out a line that moves further and further from the initial point, the motion

is said to be unstable. Liapunov has summarized this succinctly, namely: "If a point on a stable trajectory in the phase plane is perturbed slightly and if the resulting motion remains close to the original trajectory for all time, the dynamical system whose motion is represented by the trajectory is said to be stable." We chose to represent the phase plane as the total length of the perturbed velocity and its integral with respect to time for the ordinate and the abcissa, respectively. The perturbation is about the equilibrium state, which is denoted by the subscript 0. Thus the perturbed velocity vector may be written as $(u - u_0, v, w - w_0, R_t p, R_n q, R_b r)$. Here R_t, R_n, and R_b are the appropriate components of the torsion, the normal and the binormal radii of curvature of the vehicle's trajectory in physical space. If one is not interested in comparing the stability of several different systems, but rather the stability of one system under different circumstances such as gross weight, then if the equilibrium state corresponds to steady motion, if it is sufficient to represent the velocity vector as $(u - u_0, v, w - w_0, p, q, r)$ since the product of the several radii and the several angular velocities approach zero as the system approaches equilibrium. The simpler approach is adequate for the purpose of discussing stability.

Specific Application

The vehicle considered in this investigation was the Long Duration Expendable Decoy (LODED) formulated by Locus, Inc. for the Naval Research Laboratory. Data for the vehicle and its wind tunnel tests at the University of Maryland were obtained from the LODED Summary

Report[7].

Physical dimensions used were based on Figs. 1 and 2 and the supplied airplane characteristics data sheets (see Appendix A). The configuration selected was with lower winglets, wing incidence +10 degrees, tail incidence +5 degrees, and center of gravity at the balance center of the wind tunnel model. The airfoil used for the wing, tail, and winglets was the Wortman FX63-137. In addition to this, the Lissaman airfoil was used to investigate the effect of hysteresis on stability calculations. (Section lift for both cases shown in Figs. 3A and 3B).

Three methods were used to numerically model the dynamic response of the aircraft. The first is a longitudinal plane method that only solves for the velocities u, w, the flight path angle γ, the fuselage reference line angle θ, and the angle of attack α. The method used the linear stability derivatives supplied in a printout that came with the data. The equations for this method are different than those for the other two methods, and will be discussed further under the section entitled Pitch Plane. The second method used is also a linear method. It solves for the external forces and moments using linear stability derivatives, and uses these in the nonlinear equations of motion. The third method used is a fully nonlinear method. It uses strip theory to solve for the external forces and moments, and then corrects this result for real effects using a wind tunnel correction factor. Using this method the response of the vehicle at high angle of attack can be modelled. Figure 3C shows the lift coefficient for the wind tunnel test, along with the slope used for the stability derivatives. This big

difference in slope (especially at the α=0 point), the linear and nonlinear methods cannot be reliably compared if the motion varies over a wide α range.

The basic equations of motion were described above and come from Ref. 1. These equations have been modified to accommodate the pitch roll and the pitch yaw products of inertia, even though for this vehicle they equal zero. The coordinate system used was body axis, shown in Fig. 4. The controls were assumed to be fixed, so that the total number of independent equations is reduced to 9, matching the number of unknowns. The three equations to determine the position of the center of gravity at every time were also included, although they were never needed due to a fixed density assumption.

The equilibrium condition was assumed to be θ=0. It was desired to analyze the behavior at a fixed Reynolds number of 285,000. This was accomplished by varying the mass of the aircraft for different initial lift coefficients. The mass moments and products of inertia were varied only by the mass as the radius of gyration was assumed to be constant. The mass moment and products of inertia for the propeller were assumed to be zero.

Method of Solution

The nine independent equations can be put into a matrix form so that all of the variables can be solved for at the same time. Since this results in one basic first order nonlinear ordinary differential equation, the system can be solved using a marching method. The initial conditions are supplied, and the new values are calculated in

terms of the old values. This results in

$$U(n+1) = U(n) + \Delta t * \delta u$$

(where in this context U represents the matrix). It was found that a time step above 0.1 seconds caused the numerical method to be unstable, and so all the runs were made with a time increment of 0.1 seconds.

Stability Analysis

Linear Stability Analysis

Linear stability analysis was taken from Ref. 1 for both the longitudinal and lateral modes. Both were solved numerically, revealing the short period mode along with the phugoid mode. The periods for the modes were calculated, and are discussed in the linear stability derivative section.

Nonlinear Stability Analysis

Liapunov Stability analysis was used to evaluate the stability for both the linear and nonlinear methods. In the phase plane ($\dot{x}$-vs-x), if a point on a trajectory is displaced a small amount, the displaced point remains arbitrarily close to the original trajectory. The trajectory will look similar to the spiral shown in Fig. 5. The difficulty in uniquely determining the sign of each contribution is overcome by assuming continuity with increasing time.

Thrust and Propeller Effects

Assuming the propeller is constant speed, the variation in thrust depends on the instantaneous forward flight speed (V_x).

Thrust = $T_o*(1 - (V_x-u_o)/U_\infty)$

where subscript o indicates equilibrium value; u = u velocity component, U_∞ = total velocity.

Forces are developed by the propeller which are normal to its axis of rotation. This is due to the section lift characteristics of the propeller blades. Thus a "lift" (negative z-force) is generated if the propeller is at an angle of attack, α_{prop}. Similarly, a side force is generated if the propellers are in sideslip, β_{prop}. Since the propeller is at the tail of the vehicle, downwash must be accounted for; $\alpha_{prop} = .5*\alpha$ for the aircraft. Based on the usual approximations for propellors and a typical section lift curve slope is .05 (1/deg), the forces are:

$$F_{Z_p} = -.5\rho V^2 S\ (2.865)\ \alpha_{prop}$$

$$F_{Y_p} = -.5\rho V^2 S\ (2.865)\ \beta_{prop}$$

And resulting pitch and yawing moments:

$$M_p = F_{Z_p} * X_p$$

$$N_p = F_{y_p} * X_p$$

where X_p = location of propeller from c.g.

Linearized Stability Analysis of Controls-Fixed Motion

The dynamic response of the LODED vehicle was analyzed using the supplied lateral and longitudinal derivatives. The vehicle is perturbed from its equilibrium position by a triangular impulse to one of its velocity components. Its linear and angular velocities and orientation are calculated versus time. In addition, the stability determinant is expanded and the characteristic roots are obtained.

Equilibrium lift coefficients chosen were $C_L = .6$ and $C_L = 1$. For the desired Reynolds number, a lift coefficient beyond this range would have resulted in unreasonable thrust and attitude requirements. The angle of attack reported is with respect to the zero lift line, such that at $\alpha = 0$ degrees, $C_L = 0$.

The stability derivatives were assumed to be given in wind axes so an appropriate axis transformation was implemented. The stability derivatives with respect to the velocity u were calculated, found to be small and were neglected.

Longitudinal

Twelve runs were made with an input disturbance to the w velocity component or the u velocity component. The change in the velocity was such that if all the other motion variables were held fixed over the time of the disturbance, the desired change in angle of attack ($\delta\alpha$) would have resulted. Table I lists the pertinent information for each run. Four variables were plotted for each run, two over a short period ($\sim$ 3 sec.) and two over a longer period ($\sim$ 30 sec.). The long period plots were generated every second and at each pitch rate (q)

zero-crossing and not at each time increment interval (.01 sec.). Thus, these curves are not completely smooth and for qualitative purposes only. Runs for a longer period (~ 200 sec.) were to examine absolute convergence. Figures 6 and 7 show typical results. The calculated characteristics of the short period (A) and phugoid (B) modes are:

C_L = .6 θ_o = 0 deg.

(A) roots: (-.03375 + .06828i)

period: .648 sec.; time to-half-amp: .144 sec.

ω_n = .0762 (1/sec) ζ = .443

(B) roots: (-8.4399E-05 + .00317i)

period: 13.951 sec.; time to-half-amp: 57.574 sec.

ω_n = .00317 (1/sec) ζ = .027

C_L = 1. θ_o = 0 deg.

(A) roots: (-.02027 + .05485i)

period: .807 sec. time to-half-amp: .24 sec.

ω_n = .0585 (1/sec) ζ = .347

(B) roots: (-5.7193e-05 + .00318i)

period: 13.88 sec. time to-half-amp: 84.9 sec.

ω_n = .00319 (1/sec); ζ = .018

The numerical results similarly indicated dynamic stability for all conditions. As expected, the magnitude and duration of the disturbance ($\delta\alpha$) affects only the amplitude of motion, not its damping or frequency (period). There is agreement in that the short period and phugoid period increase with a higher lift coefficient, the former more than the latter. However, both periods were shorter in the numerical solution

than the periods obtained from the characteristic roots. From the runs at C_L=.6, the short period ~ 0.47 sec. and at C_L=1, the short period ~ .57 sec. At C_L=.6, the phugoid ~ 10.1 sec., at C_L=1, the phugoid ~ 10.08 sec.

The differences may be caused by employing a flight condition different from that at which the stability derivatives were calculated. This includes the Reynolds number, density, mass, and geometry (wing incidence, tail incidence). The effect of each of these parameters on the stability derivatives must be analyzed. Inclusion of the previously neglected u-derivatives and revised modeling of the thrust variation should be considered in any further runs.

Lateral

A perturbation to the v-velocity component was initiated to develop a sideslip, β. Two runs were performed, one at each lift coefficient. The calculated characteristics of the dutch roll (A) and spiral divergence (B) modes are:

C_L = .6, θ_o = 0 degrees

(A) root: (-.92835 + 0i) time to-half-amp: .052 sec.

root: (-.03531 + .2037i)

period: 2.17 sec. time to-half-amp: 1.375 sec.

ω_n = .207 (1/sec) ζ = .171

(B) root: (.0061 + 0i) time to-double-amp: 8.01 sec.

C_L = 1, θ_o = 0 degrees

(A) root: (-.5589 + 0i) time to-half-amp: .087 sec.

root: (-.0198 + .160i)

period: 2.77 sec. time to-half-amp: 2.45 sec.

ω_n = .161 (1/sec) ζ = .1231

(B) root: (.0059 + 0i) time to-double-amp: 8.26 sec.

It was noted that for both lift coefficients the spiral mode is divergent. That is, ψ increases continually and is not converging to any particular heading. Due to the large value of damping in roll, the rolling mode converges quickly and is not discernible in the results. The period of the "dutch roll" mode from the motion is ~ 0.75 seconds for C_L=.6, and ~ .8 seconds for C_L=1; again shorter than the period derived from the characteristic roots but still following the same trend: longer periods at higher lift coefficients.

In both runs, the longitudinal mode became excited after a lateral disturbance. A cross-coupling between the two modes of motion arose because the use of the NACA stability axes for computing derivatives. Thus the angular velocities are transformed between body and stability axes. This coupling is absent in the longitudinal disturbances only because the reference (equilibrium) sideslip is zero. This is not a problem if one uses the body axes consistent for the calculations of the stability derivatives. In the linear regime this is sufficient to "de-couple" the modes.

Pitch Plane Solution

The second method of solution used to study the dynamic response of the aircraft was one which just considered the motion in the pitching plane. The standard equations are used (Ref. 1, pp. 181-185) except that the actual variation of C_L with angle of attack was used. They

were solved by a backwards differencing technique which yields:

$$I\theta = G$$

$$\theta(n+2) = \theta(n+1) \times 2. - \theta(n) + \Delta t^2 \, G/I$$

The time step used was 0.05 seconds. For time increments larger than this, the numerical method was unstable. Table II shows the cases that were run. Using this method, the aircraft is stable for all disturbances used.

The phugoid period of the calculated motion was ~ 22 sec. This was significantly longer than the value calculated from the stability derivatives. All variables demonstrated extreme sensitivity to disturbances to the pitch angle θ.

The Nonlinear Method

Strip Theory

In order to calculate the external forces and moments acting on the aircraft, strip theory was used. This involves calculating the local angle of attack at each strip along the surface (surface being either wing, tail or winglet), and integrating the contribution over the entire span. The section characteristics are assumed valid at each strip. Wind tunnel data and section characteristics were curve-fitted using IMSL subroutines at the Joint Computer Facility. Average error for each fit was below 6%. Longitudinal force and moment coefficients (C_L, C_D, C_M) were assumed symmetric for positive and negative sideslip while the lateral coefficients (C_Y, C_l, C_N) were assumed anti-symmetric.

The local velocity at each point was given by the following

equations,

$$\text{if } v = u + \omega \times r$$

$$v_x = u + qz - ry$$

$$v_y = v + rx - pz$$

$$v_z = w + py - qx$$

which leads to local angle of attack of:

$$\alpha = \tan^{-1} v_z/v_x$$

and aircraft angle of attack:

$$\alpha_o = \tan^{-1} w/u$$

The velocity at each point is now:

$$V = v_x^2 + v_y^2 + v_z^2.$$

For the wing, the local angle of attack is:

$$\alpha = \tan^{-1} v_z/v_x + i_w$$

Using the velocity at each point, the thrust now uses the velocity Vx which accounts for the distance away from the center of gravity.

The angle of attack at the tail included two correction factors. The first takes care of the time lag from wing to tail, and the second takes care of the downwash at the tail. This results in the angle of attack at the tail being given by the following equation:

$$\alpha = 1/2\ (\tan^{-1}(v_z/v_y)) + i_t$$

The angle of sideslip is given by:

$$\beta = \tan^{-1}\ (v_y/v_x)$$

Since the winglets are the same airfoils as the wing and tail, the above angle is used to get a side force from the CL-vs-α curve. Note that although the winglets are at a different Reynolds number than the

wing and tail, insufficient data exists to correct for this factor.

In order to correct strip theory for real effects (interference with fuselage, induced velocities, etc.) a wind tunnel correction factor was included. This factor, R, was equal to the wind tunnel results divided by the strip theory results if the angular velocities are zero. The equations for the external moments and forces become:

EXTERNAL FORCE (OR MOMENT) REAL =

EXTERNAL FORCE (OR MOMENT) STRIP THEORY X

(EXTERNAL FORCE (OR MOMENT) WIND TUNNEL)/

(EXTERNAL FORCE (OR MOMENT) STRIP THEORY WITH NO ANGULAR VELOCITY)

The equations were solved numerically using the trapezoidal rule. The contribution to the force or moment was evaluated at two points, averaged, and then applied at the strip between them. The fuselage contribution is given by the method previously discussed (Appendix C). The type of disturbance used is the same as that described in the linear section.

Runs Using Strip Theory

A summary of runs is listed in Table III. Detailed plots and all computer printouts are available upon request.

Discussion of Strip Theory Results

Typical plots are given in Figure 8. A few general trends can be identified. In the short period mode, period about .1 sec., variations in angle of attack are a function of both the disturbance magnitude and duration. The period is only slightly dependent on the magnitude, while very dependent on the duration. For longer duration of the disturbance,

the period is more affected by the magnitude than in the case of the shorter duration. When the initial angle of attack is in the nonlinear range, the period becomes slightly longer, on the order of 5%.

The damping in the short period mode is relatively unaffected by the magnitude of the disturbance, although it does seem more damped for longer duration of disturbance. As expected, the damping in the nonlinear range is less than that in the linear range. In general, in both linear and nonlinear regions, the longer duration disturbance is more heavily damped.

The long period mode, the phugoid, is generally lightly damped. This is in contrast to the short period mode which is generally very heavily damped. In the nonlinear region, this trend no longer is seen. Instead the short period mode is lightly damped, while the phugoid is the more heavily damped. Although the amplitude in the nonlinear range is altered by the non-linear effect, the period is relatively independent as expected. For both cases the period phugoid is about 10 seconds, about 30% less than the linear analysis prediction, which is frequently the case (Ref. 1).

Liapunov stability indicates that the aircraft is unstable, primarily due to the spiral instability mode. Originally the phase plane plot indicates a stable spiral (Figs. 9-16). As time goes on, the trajectory starts to move out away from the origin. Since we did not suppress the lateral modes, they appeared following the disturbance of the longitudinal mode. All runs showed this instability, but to varying degrees. This can be explained by noise and round-off error, which is

amplified in the unstable lateral mode.

Figures 9, 10, 11 show the effect of input disturbance upon the Liapunov stability for lift coefficient of 2.33. Generally speaking the results are similar (although three different scales were used to illustrate the following patterns). Figure 9, the small perturbation, behaves nearly the same way as the motion resulting from linear aerodynamics. The larger disturbance pushes the aircraft near the stall so the amplitude increases and the damping is reduced. Note some saturation on the plotter is evident earlier in Figs. 10 and 11. The drift into the lateral instability always occurs at about the same distance.

Figures 12, 13, 14 show the effect increasing the equilibrium lift coefficient to 2.77. Here the motion proceeds past stall, and the motion is less oscillatory, i.e., the "spring strength" is reduced. In fact the oscillation fails to build up before the lateral instability builds up.

Figure 15 shows a lateral stability run, with a lightly developed Dutchroll and which also shows strong spiral divergence.

Figure 16 shows the hysteresis loop (Fig. 3c) effects which shows a pitch oscillation that is lightly damped. It suggests that without care, the hysteresis could be coupled with dynamics for a new class of instability.

The Lissaman (Fig. 3c) airfoil was used due to an "interesting" hysteresis loop in stall. Since the aircraft was not tested with this airfoil, there is not an appropriate wind tunnel correction factor. It

was felt that the correction factor for the FX-Wortman airfoil would be better than no correction at all. The only change made was in the incidence of the wing and tail. They were changed at each initial angle of attack of the aircraft so that they would reach the bottom loop at the disturbance. This was done so that the airfoil would be running in the range of the hysteresis loop. Note that the value of mass and equilibrium thrust wre calculated for the FX-Wortman.

The Lissaman airfoil was run under initial conditions that were very close to the upper angle of attack end of the lift curve. The angle of attack was then perturbed in the negative direction, causing the reaction to drive it to the lower hysteresis loop. Due to the nature of the algorithm, once there it was never able to reach the upper curve again. Hence this result represents oscillation into a stall regime. Results for the Lissaman airfoil are somewhat different from those for the Wortman airfoil. The short period mode with the Lissaman airfoil is longer than that with the Wortman, while the phugoid appears to be slightly smaller.

Due to lack of time, only one lateral run was made. The side slip velocity appeared to damp out very rapidly. The short period mode seemed longer than that in the longitudinal case, although it was not plotted for long enough to positively confirm this. The long period mode has a period of about 5 sec., which is half as short as that in the longitudinal case. The Liapunov stability analysis revealed a slowly decreasing velocity and a rather rapidly increasing distance. This, along with the printout for the heading angle, seems to indicate

that the aircraft is seeking a new heading, i.e., the machine possesses a spiral, instability, or predicted by the linear theory.

Low Reynolds Number Data

It is perhaps worth noting that aerodynamic data that is obtained at low Reynolds numbers may lack the precision and repeatability of that taken at higher Reynolds numbers. There are several reasons for this difficulty. First the dynamic pressures are lower so the size of the forces and moments that are being measured are lower. This in and of itself creates difficulties. Secondly, extensive regions of laminar flow may exist which are more prone to separation or sensitivity to surface conditions than turbulent boundary layers. Thirdly, the transition region seems to be much longer than it is at higher Reynolds number, and there is inherent uncertainty introduced by these transition effects. As Mueller has pointed out[10], the free stream disturbances can have an unduly large influence on the accuracy and repeatability of data measured at low Reynolds numbers. Finally, there is practically no dynamic stability data at all. Because of the problems of taking steady state data, and because of the unknown effects of unsteady flow on these stability derivatives, estimated values must be treated with care. These effects include the possibility that one cannot uncouple the lateral motion from the longitudinal motion in performing the stability analysis, particularly when non-linear aerodynamic characteristics need to be used.

Conclusions

Not unexpectedly the usefulness of the linearized stability analysis is limited when applied to flight at high lift coefficients at low Reynolds numbers. The concept of local linearizations may well be useful as long as $\delta\alpha$ is limited, that is, it be the matter of

$$\text{(A)} \quad |\delta\alpha| << \frac{2\left.\frac{dc}{d\alpha}\right|_{\alpha o}}{\left.\frac{d^2C_L}{d\alpha^2}\right|_{\alpha o}}$$

$$\text{(B)} \quad |\delta\alpha| << \frac{2\left.\frac{dC_M}{d\alpha}\right|_{\alpha o}}{\left.\frac{d^2C_M}{d\alpha^2}\right|_{\alpha o}}$$

Where these conditions are violated, then the linear theory overestimates both the frequency of the motion (i.e., the period is too short) and the damping (i.e., δ is too large) when compared to solutions of the equations of motions. Further in the non-linear lift regime lateral motions will feed into the longitudinal motion. The converse is not as evident. The hysteresis in the lift curve can couple into the motion unfavorably. The local increase in stiffness coupled with a drastic reduction in damping could lead to divergent motions in pitch.

The use of a generalized phase plane is indicative of an instability. However this technique is no more efficient than any

trajectory integration scheme. It's virtue is its compactness of the results it presents.

The clearest need from this study is that of additional reliable data in this Reynolds number range. It is needed in several forms:

(1) Static Aerodynamic Characteristics;

(2) Dynamic stability derivatives measured with small amplitude at a variety of set points; and

(3) Some trajectory simulation data using a dynamic, perhaps a magnetic model suspension system, to probe for unexpected, non-linear aerodynamic coupling.

The dynamic response of the LODED vehicle was modeled three different ways. All methods that indicated the lateral resonse were unstable. Liapunov stability analysis proved to be a useful way of determining the stability (or instability) of the system for both linear and nonlinear models. Strip theory with a wind tunnel correction factor was successfully used to calculate external forces and moments for the full nonlinear control fixed equations. Further investigation is needed to resolve the longitudinal/lateral coupling, to fully determine the effects of a hysteresis loop and also to completely analyze the results. The aerodynamic data should be further correlated to provide compatability among the three methods of investigations.

Conclusions and Recommendations

References

1. Etkin, Bernard; Dynamics of Flight, 2nd ed.; John Wiley and Sons; New York, NY, 1982.

2. McCormack, Barnes W.; Aerodynamics, Aeronautics, and Flight Mechanics; John Wiley and Sons; New York, NY, 1979.

3. Durand, W.F., ed.; Aerodynamic Theory, Vol. 5, Section N, "Dynamics of the Airplane" by B.M. Jones; Springer Verlag, Berlin, 1934.

4. Durand, W.F., ed.: loc. cit. ante,. Vol. 4, Section J. "Applied Airfoil Theory" by A. Betz; pp. 94-129.

5. Winkleman, A., and Barlow, J.B.; "Flowfield Model for a Rectangular Planform Wing Beyond Stall"; AIAA Journal, Vol. 18, No. 8, pp. 1006-08, August 1980.

6. Schrenk, Otto; "A Simple Approximation for Obtaining the Spanwise Lift Distribution," NACA TM 948, 1940.

7. Eklund, R.C., LODED Summary Report: FY-78 through FY-81, Vol. I and II; Locus, Incorporated, State College, Pennsylvania.

8. LaSalle, Joseph, and Lefschetz, Soloman; Stability of Liapunov's Direct Method; Academic Press, New York, 1961.

9. Schlicting, H. and Truckenbrodt, E.; Aerodynamics of the Airplane; McGraw-Hill Company, New York, NY, 1979.

10. Mueller, T.J., Pohlen, L.J., Conigliaro, P.E. and Jansen, B.J., Jr.; The Influence of Free Stream Disturbances on Low Reynolds Number Airfoil Experiments; Experiments in Fluids, V.1, No. 1, P1; Springer-Verlag, 1983.

APPENDIX A (Ref. 7)

Vehicle: Loded GW=140 LBS, CG=19.8 inches aft of fwd pivot - CG1
Lower winglets with wing pivots at .32 chord (calc. & meas. der)

Pertinent Airplane Characteristics

Density (slugs/ft**3)	= 0.00237	Velocity (ft/sec)	= 71.000
Mass (slugs)	= 4.350	IYY (slug-ft**2)	= 13.89
Thrust (pounds)	= 0.000	ZJ (ft)	= 0.000
GCOS (gamma) (ft/sec/sec)	= 32.200	GSIN (gamma) (ft/sec/sec)	= 0.000
COS (XZ)	= 0.999	SIN (XZ)	= 0.052
Wing Area (ft**2)	= 10.000	Horiz. Tail Area (ft**2)	= 10.000
Wing Span (ft)	= 10.000	Horiz. Tail Span (ft)	= 10.000
Wing Chord (ft)	= 1.000	Horz. Tail Chord (ft)	= 1.000
Wing Aspect Ratio	= 10.000	Horz. Tail Aspect Ratio	= 10.000
Wing Taper Ratio	= 1.000	Horz. Tail Taper Ratio	= 1.000
Wing Alpha (degrees)	= 21.800	Tail Alpha (degrees)	= 6.667
IWing (degrees)	= 16.000	ITail (degrees)	= 6.000
Downwash Angle (degrees)	= 5.133	Downwash/Alpha	= 0.127
Elevator Angle (degrees)	= -5.306	Elevator Area (ft**2)	= 4.800
Tail Efficiency	= 1.000	Elevator Chord (ft)	= 1.000
2-D Wing CLA	= 0.040	2-D Tail CLA	= 0.113
CDO	= 0.050	2-D Wing CDA	= 0.191
2-D Wing CL	= 1.775	Wing CMAC	= -0.076

Distances

Length of Fuselage (ft)	= 7.000
Width of Fuselage (ft)	= 1.000
C.G. to Tail Quarter Chord (ft)	= 2.470
Wing to Tail Quarter - Chord (ft)	= 4.167
C.G. to Wing A.C. (chordwise) (ft)	= 1.330
C.G. to Wing A.C. (vertical) (ft)	= -0.410
Nose to Wing Quarter - Chord (ft)	= 1.043
C.G. to Wing Quarter - Chord (ft)	= -1.690
C.G. to Thrust Axis (ft)	= 0.0000

Longitudinal Stability Derivatives

CL = 2.3000	CLA = 4.0110	CLAD = 5.4581	CLQ = 18.3339
CD = 0.2320	CDA = 1.1170	CDAD = 0.0000	CDQ = 0.0000
CM = 0.0000	CMA = -9.3910	CMAD = -13.4815	CMQ = -74.8187
CLDE = 2.7690	CLU = 0.0000	CT = 0.0000	
CDDE = 0.7000	CDU = 0.0000	CTU = 0.0000	
CMDE = 4.6100	CMU = 0.0000	CTRPM = 0.0000	

4.79006	0.76236	52.99	34.48468	-0.90265	-51.71787
5.74807	0.91483	60.52	35.63810	-1.37764	-78.93292
6.38675	1.01648	58.59	35.35603	-1.76333	-101.03116
7.02542	1.11813	50.47	34.06121	-2.11651	-121.26698
7.98344	1.27060	36.55	31.25798	-2.49515	-142.96154
10.00000	1.59155	19.49	25.79523	-2.89862	-166.07883
100.00000	15.91549	0.40	-7.95587	-4.34941	-249.20278
1000.00000	152.15494	0.04	-28.45762	-4.67488	-267.85109

Vehicle: Loded GW=140 lbs, CG=19.8 inches aft of fwd pivot - CG1
Lower winglets with wing pivots at .32 chord (calc. & meas. der)

Pertinent Airplane Characteristics

Rho = 0.00237 Wing Area = 10.00 Mass = 4.35 GCOS (gamma) = 32.20
U = 71.00 Chord = 1.000 Span = 10.000 GSIN (gamma) = 0.000

IXX = 10.1	IXZ = 0.54	IZZ = 22.6	CLW = 1.4792
SA = 0.000	DIH = 0.000	ZC = 0.450	FUSVOL = 7.417
H = 1.182	SV = 1.275	BV = 1.670	R1 = 0.569
TR = 1.000	ZV = 0.055	ETAV = 1.000	SBS = 7.338
LF = 7.000	LTV = 2.544	XM = 2.775	H1 = 1.000
H2 = 1.000	WFUS = 1.000	SAH = 0.000	CLA2DW = 0.040
BH = 10.000	SH = 10.000	TRH = 1.000	CLA2DH = 0.113
BA = 4.500	CA = 1.000	SR = 0.000	ALPHAR = 5.800
CDO = 0.050	YI = 0.500	HNOSE = 1.000	WNOSE = 1.000

HFCY = 1.0000 WFCY = 1.0000 LFCY = 4.7467 LMH = 4.7470
HBCY = 1.1380 WBCY = 1.0000 LBCY = 6.0000

Lateral Stability Derivatives

CYB = -0.9740	CℓB = -0.0888	CNB = 0.0962
CYP = 0.1150	CℓP = -1.1400	CNP = -0.1233
CYR = 0.4168	CℓR = 0.4040	CNR = -0.0513
CYDA = -0.0810	CℓDA = 0.9773	CNDA = -0.0138
CYDR = 0.0000	CℓDR = 0.0000	CNDR = 0.0000

Response to Aileron Deflection

CYIN = -0.081000 CℓIN = 0.977300 CNIN = -0.013800 K = 2 ACC = 0.001000

Dimensional Stability Derivatives

YV = -0.18839 ℓB = -5.25247 NB = 2.54455

APPENDIX B

Modeling of Fuselage for Stability Derivatives

The contribution of the fuselage to the external forces and moments is required in the strip theory method. The aerodynamics of the fuselage are developed from potential flow and revised for the effects of viscosity.

The pressure distribution on an inclined fuselage by the method of dipole distribution yields:

$$C_p(x,\nu) = -2 \frac{\cos\nu}{R(x)} \frac{d}{dx} (\alpha(x)\ R^2(x))$$

Integration over ν results in the lift of length dx for the fuselage:

$$\frac{dL}{dx} = 2\pi q_\infty d(\alpha(x)\ R^2(x))/dx$$

For non-circular cross-sections, the semi-width, $b_f(x)/2$, is substituted for R(x). Thus, after integration

$$L_F = 2\pi q_\infty (\alpha(x)\ b_f^2(x)/4)\Big|_o^{l_f}$$

$$L_F = (\pi/2)\ q_\infty b_{f_{l_f}}^2\ \alpha_{l_f}$$

where subscript l_f indicates evaluation at tail of fuselage.

The pitching moment is obtained:

$$M_F = \int_o^{l_f} - \frac{dL_F}{dx} x \, dx$$

$$M_F = (\pi/2) \int_o^{l_f} q_\infty \alpha(x) \, b_f^2(x) \, dx$$

For a first approximation, assume $\alpha(x)$ is constant along the fuselage and equal to at the c.g.

The lift and pitching moment for the LODED fuselage are obtained with the appropriate width distribution, $b_f(x)$. The drawings of the fuselage indicate it is not a completely closed body at the tail (exclusive of the propeller) with $B_f \approx 6$ inches. According to Hafer[9], viscous effects can be accounted for by using the geometric width plus the boundary-layer displacement thickness, $\delta(x)$, as the actual width in the equations.

From these considerations the fuselage can be approximated: Thus,

$$L_F = (\pi/2) \, q_\infty \alpha (1)^2$$

and integration of Eq. 4:

$$M_F = (\pi/2) \, q_\infty \alpha \left[-\frac{4}{3} x^3 + 4rx^2 \right] \Big|_o^r + x \Big|_o^{l_f}$$

substitution of proper values:

$$M_f = (6.58333) \, (\pi/2) \, q_\infty \alpha$$

At zero angle of attack, the drag on the fuselage is nearly equal to the drag on a flat plate of equal surface area and length. From

Ref. (2)

$$D_F = D_{\substack{\text{flat}\\\text{plate}}} (1 + (.5)\delta_F) \qquad (\alpha=0^\circ)$$

$$\text{with} \quad \delta_F = \frac{b_{fmax}}{l_f} = 1 \text{ ft./7 ft.}$$

$$D_{\substack{\text{flat}\\\text{plate}}} = C_f S_F q_\infty$$

With Reynolds number for the fuselage = $285{,}000 \times l_f/c = 1{,}995{,}000$, the friction factor = .0064.

$$S_F = 2\pi r^2 + (l_f - r)(b_{fmax})$$

$$S = 27.5708 \text{ ft.}$$

According to Wieselberger[2], the induced drag on an inclined fuselage is estimated:

$$D = \frac{1}{2} \frac{L_F^2}{\rho V^2 \pi} \frac{B^2}{(B^2 - b_{fmax}^2)^2} \qquad B = \text{semi span} = 5 \text{ ft.}$$

Thus the total drag on a fuselage at an angle of attack:

$$D_F = c_f S_F (1+(.5)\delta_F) q_\infty + \frac{1}{2} \frac{L_F^2}{\rho V^2 \pi} \frac{B^2}{(B^2 - b_{fmax}^2)^2}$$

Substitution of appropriate constants leads to:

$$D = (.1888) q_\infty + (3.9788736) \frac{L_F^2}{\rho V^2}$$

The side force, Y, and yawing moment, N, are dependent upon the sideslip angle, β, and are modeled analogously to the lift and pitching moment, respectively:

$$Y_F = -(\pi/2)q_\infty\beta$$

$$N_F = -(6.58333)\ (\pi/2)\ q_\infty\beta$$

Equations 5 to 9 are implemented in the program.

TABLE I
RUNS FOR LINEARIZED ANALYSIS

RUN #	$\delta\alpha$	δu, δv, δw, needed	Time of Disturb.	ΔMATRIX= $\frac{\delta u}{\delta t}$, $\frac{\delta r}{\delta t}$, $\frac{\delta w}{\delta t}$	δt = .01 sec Variables Plotted Short Period	Long Period
	C_L = 1.0	θ_o = 0°		α_o = 14.285°		
1	+1°	δw = 1.286	.1 sec	128.556	α, θ	u, q
2	+1°	δw = 1.286	.5 sec	128.556	α, θ	u, θ
3	+2°	δw = 2.582	.1 sec	258.244	α, θ	u, θ
4	+2°	δw = 2.582	.5 sec	258.244	α, θ	u, q
5	+4°	δw = 5.217	.1 sec	521.71	α, q	u, θ
6	+4°	δw = 5.217	.5 sec	521.71	α, q	u, q
	C_L = .6	θ_o = 0°		α_o = 8.571°		
7	+1°	δu = 7.454	.1 sec	-745.44	α, θ	u, θ
8	-1°	δw = -1.249	.5 sec	-124.955	α, q	u, q
9	+2°	δw = 2.521	.1 sec	252.111	α, θ	u, θ
10	+2°	δw = 2.521	.5 sec	252.111	α, q	u, θ
11	-4°	δw = -4.97	.1 sec	-496.804	α, q	u, q
12	+4°	δu = -22.76	.5 sec	-2275.704	α, q	u, q
Lateral						
	C_L = 1.0	θ_o = 0°		β_o = 0°		
13	$\delta\beta$ = +1°	δv = 1.201	.5 sec	120.1	β	ψ
	C_L = .6	θ_o = 0°		β_o = 0°		
14	$\delta\beta$ = +4°	δv = 4.91	.1 sec	490.935	β, p	β, ψ

TABLE II
RUNS FOR PITCH-PLANE ANALYSIS

RUN #	Duration of Disturbance	ΔDisturbance = $\delta\theta/\delta t$	δt = .005 sec
	C_L = .6	θ_o = 0°	
1	.1 sec	1.0	
2	.1 sec	5.0	
5	.5 sec	1.0	
6	.5 sec	5.0	
	C_L = 1.0	θ_o = 0°	
3	.1 sec	1.0	
4	.1 sec	5.0	
7	.5 sec	1.0	
8	.5 sec	5.0	
9	.5 sec	-5.0	
10	.1 sec	-5.0	

TABLE III
STRIP THEORY RUNS

RUN #	C_L	Δt	$\delta(\alpha_{cal})$	$\delta(\beta_{cal})$
1	2.33	.1	1°	0°
2	2.33	.1	2°	0°
3	2.33	.1	4°	0°
4	2.33	.5	1°	0°
5	2.33	.5	2°	0°
6	2.33	.5	4°	0°
7	2.77	.1	1°	0°
8	2.77	.1	2°	0°
9	2.77	.1	4°	0°
10	2.77	.5	1°	0°
11	2.77	.5	2°	0°
12	2.77	.5	4°	0°
13	2.33	.1	0°	2°
14 Lissaman	2.33	.1	-1°	0°

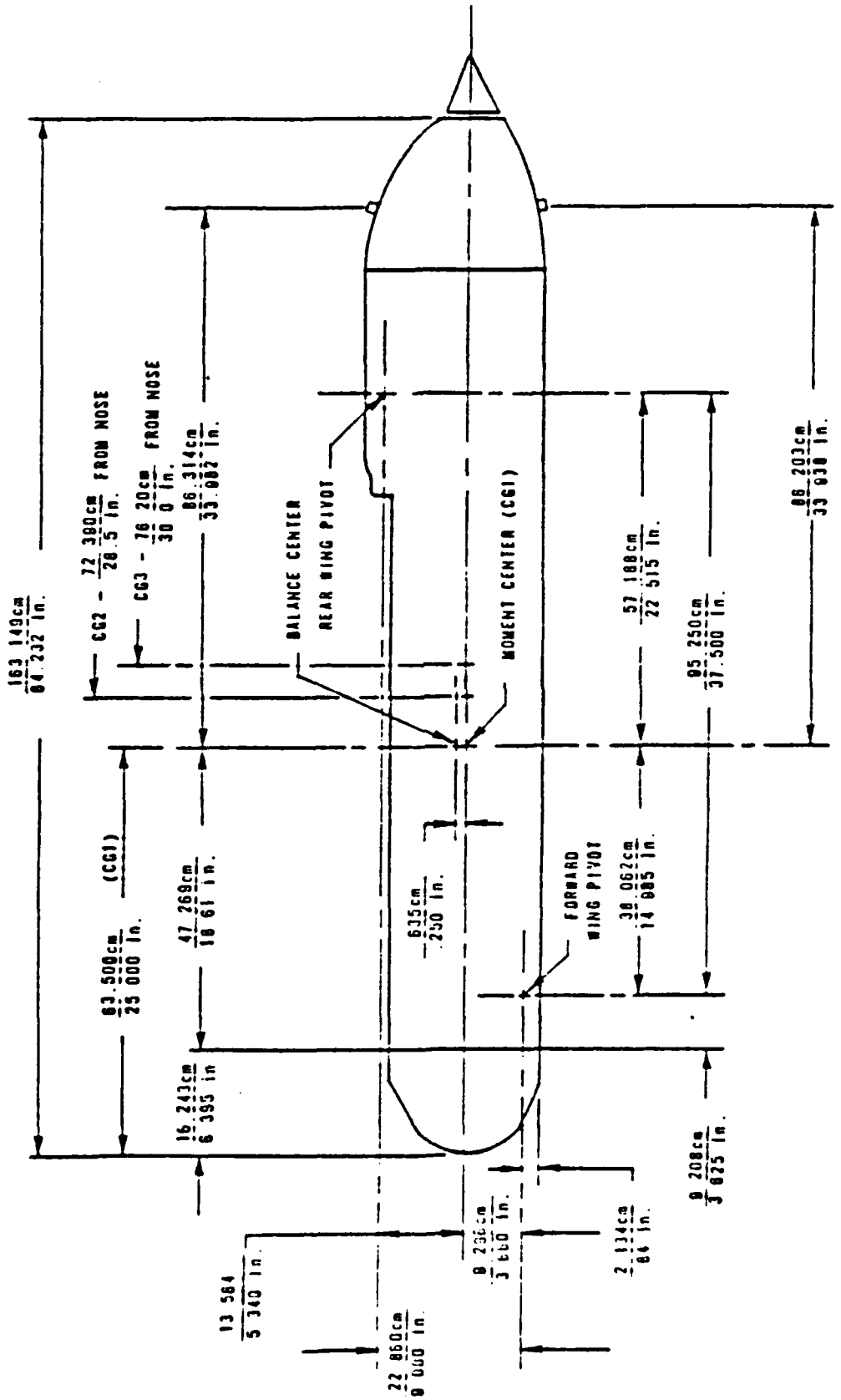

FIG. 1 DETAILS OF LODED FUSELAGE GEOMETRY

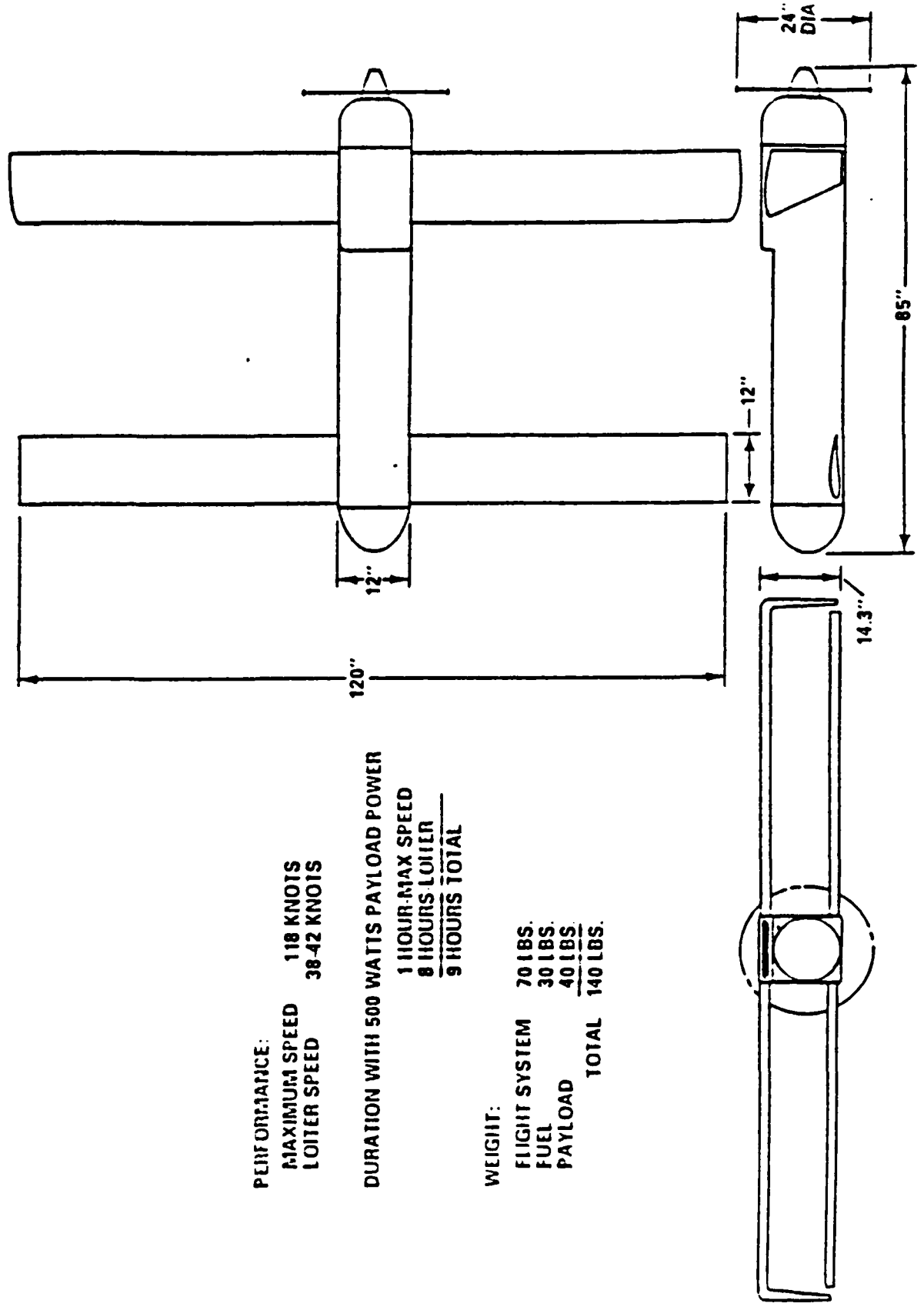

FIG. 2 LONG DURATION EXPENDABLE DECOY

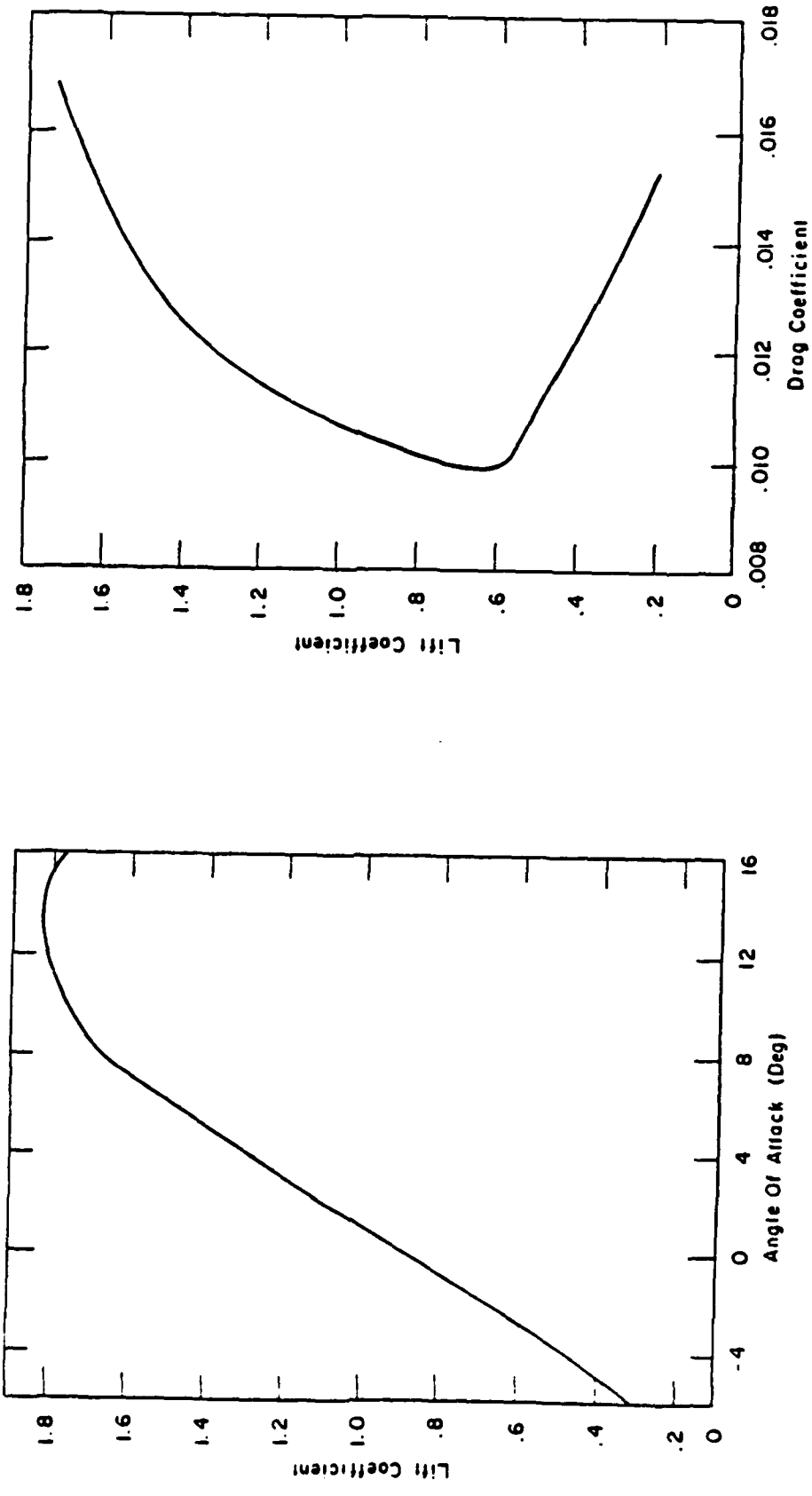

FIG. 3A WORTMAN FX 63-137 AIRFOIL, SECTION CHARACTERISTICS

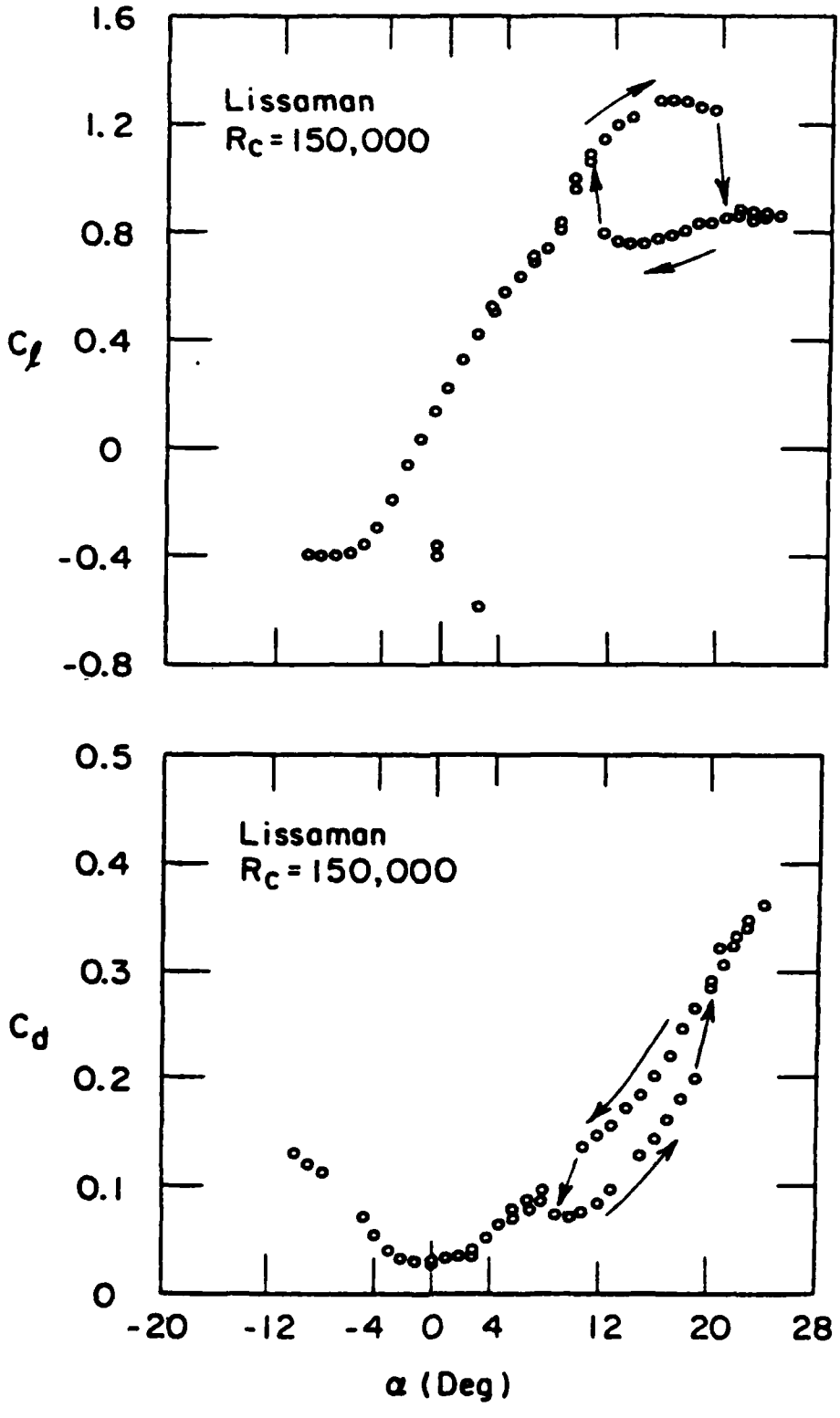

FIG. 3B LISSAMAN AIRFOIL, SECTION CHARACTERISTICS

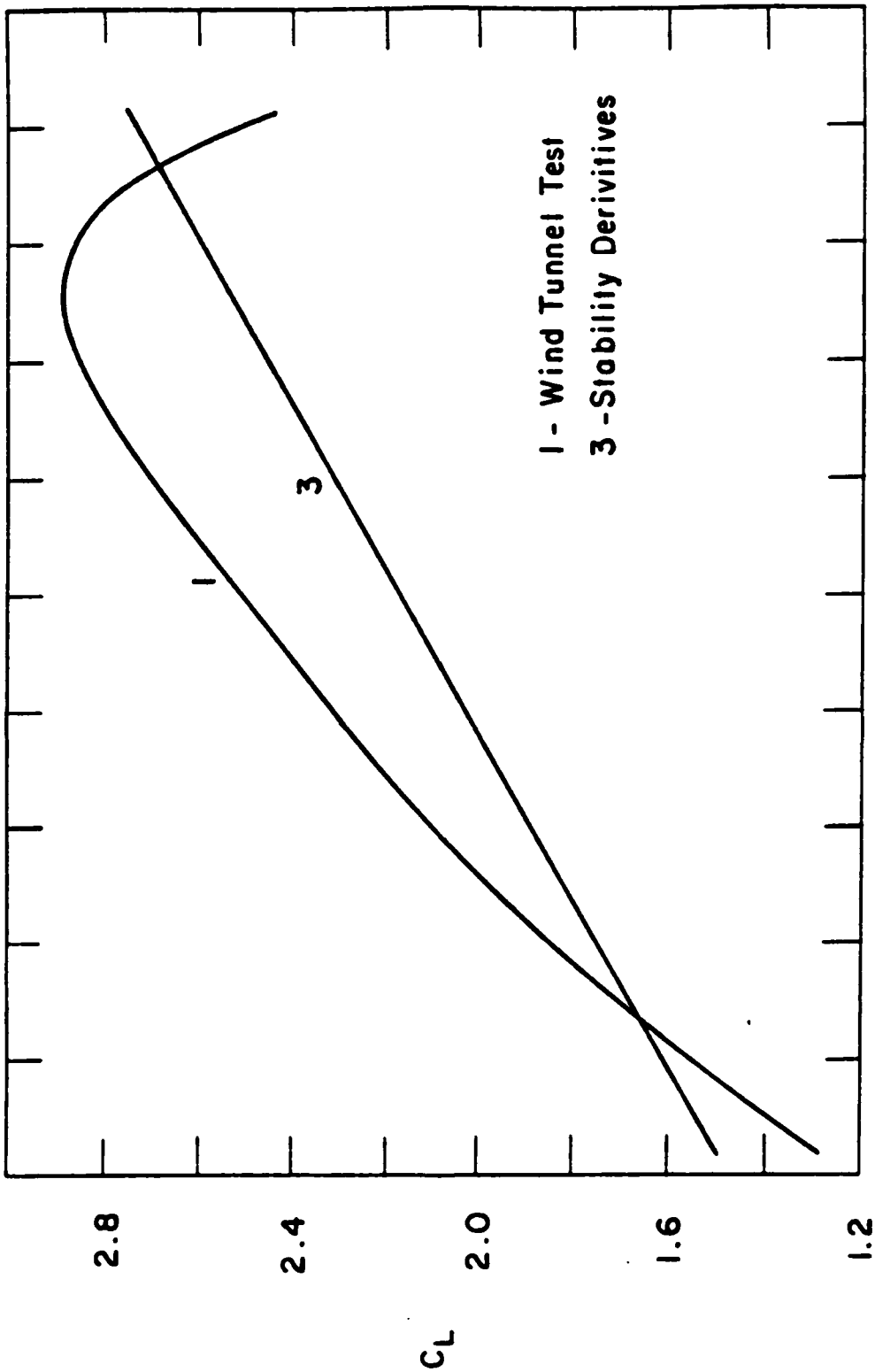

FIG. 3C COMPARISON OF LIFT CURVE FOR STABILITY DERIVATIVE AND MEASURED LIFT CURVE

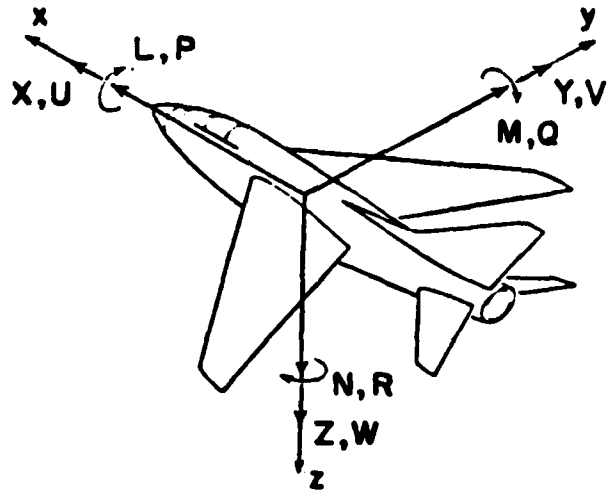

FIG. 4 COORDINATE SYSTEM

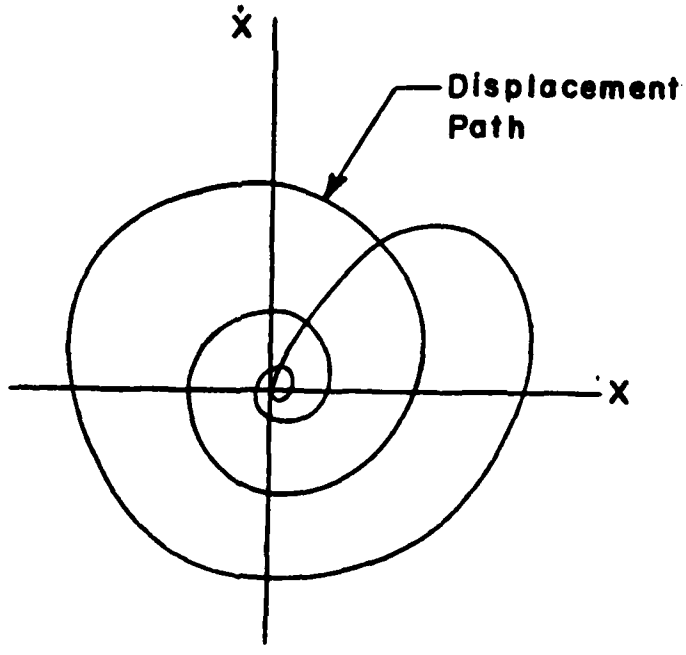

FIG. 5 PHASE PLANE - A STABLE SPIRAL

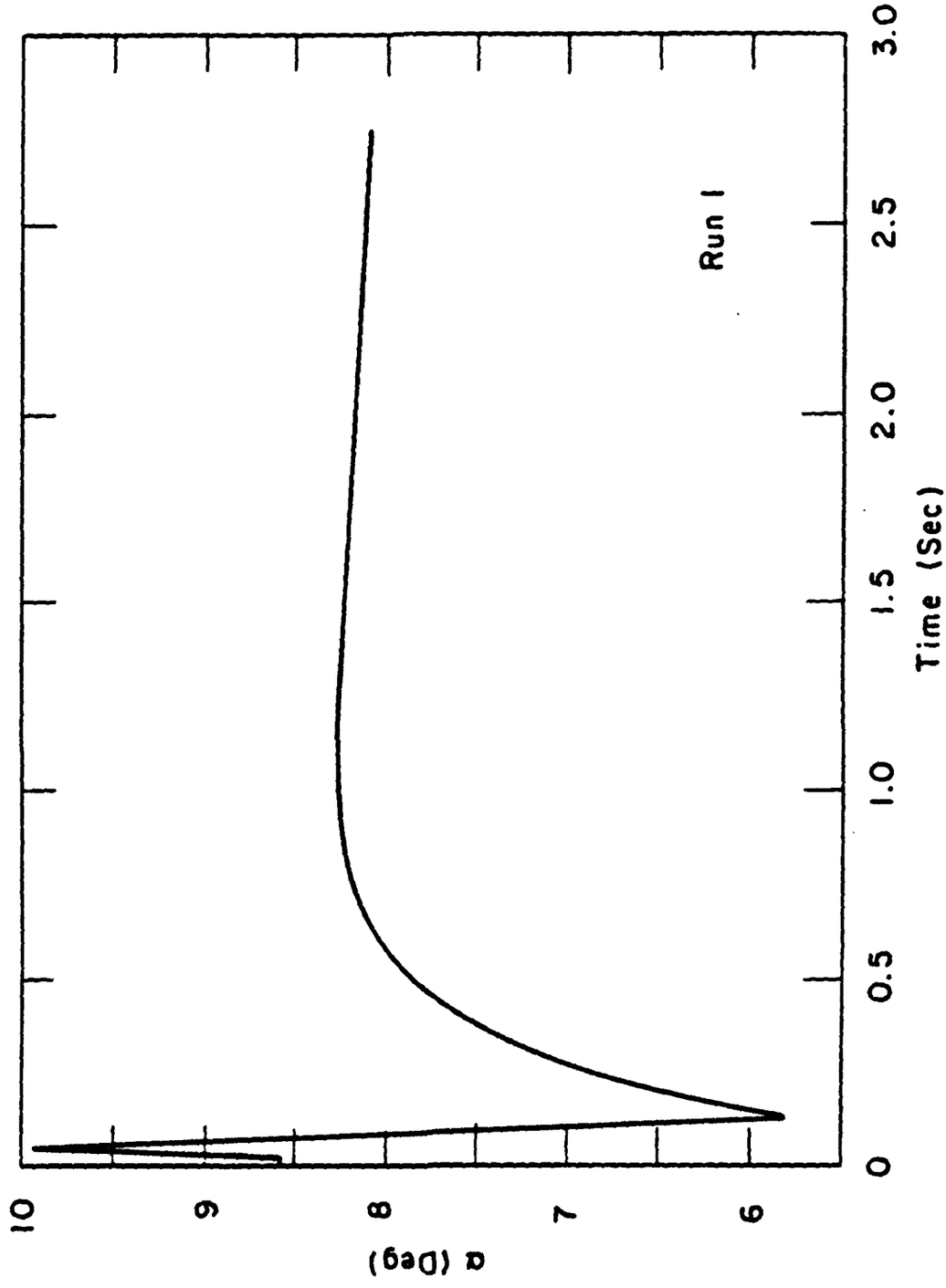

FIG. 6 SHORT PERIOD MOTION (LINEARIZED)

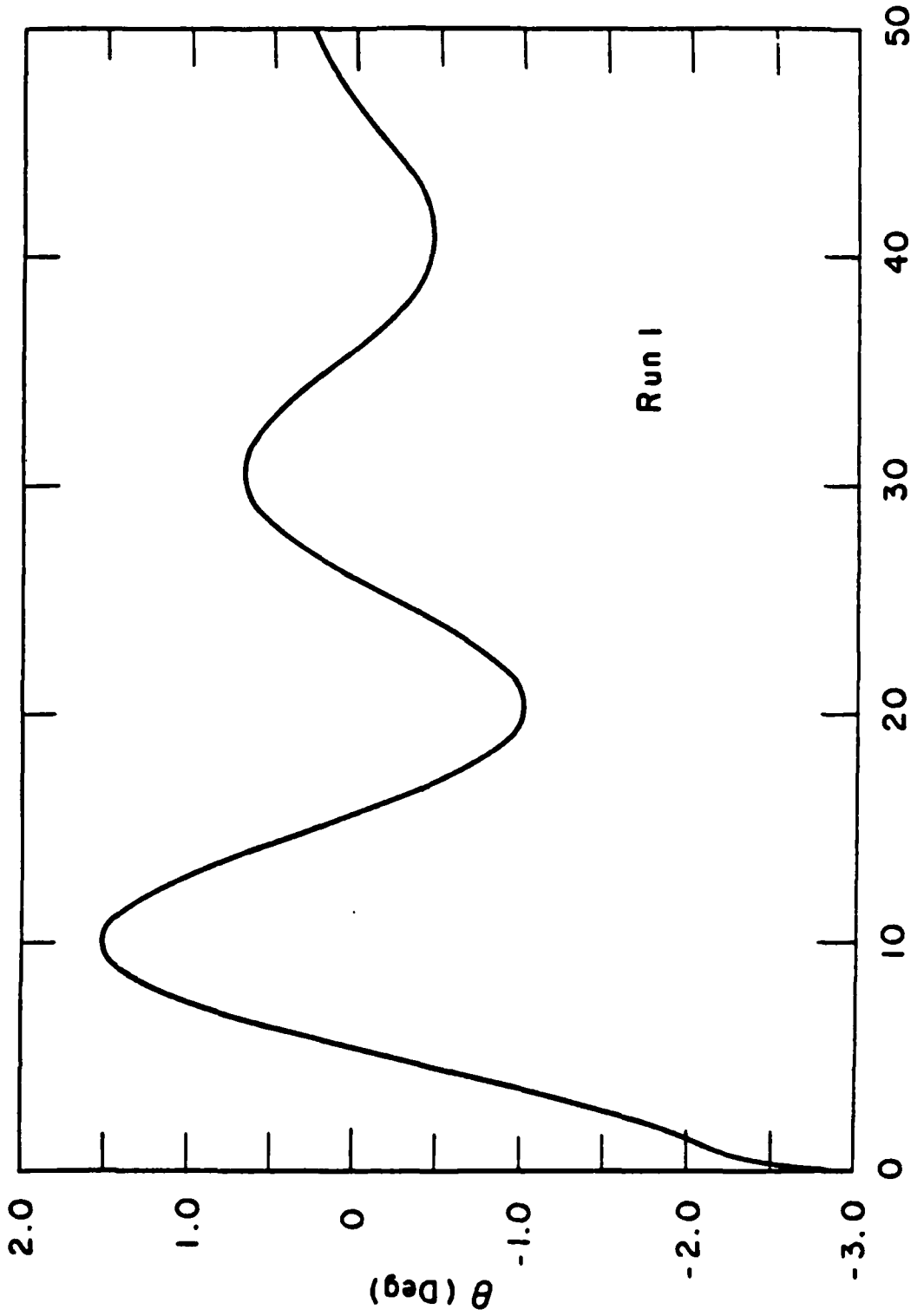

FIG. 7A VELOCITY PITCHING MOTION

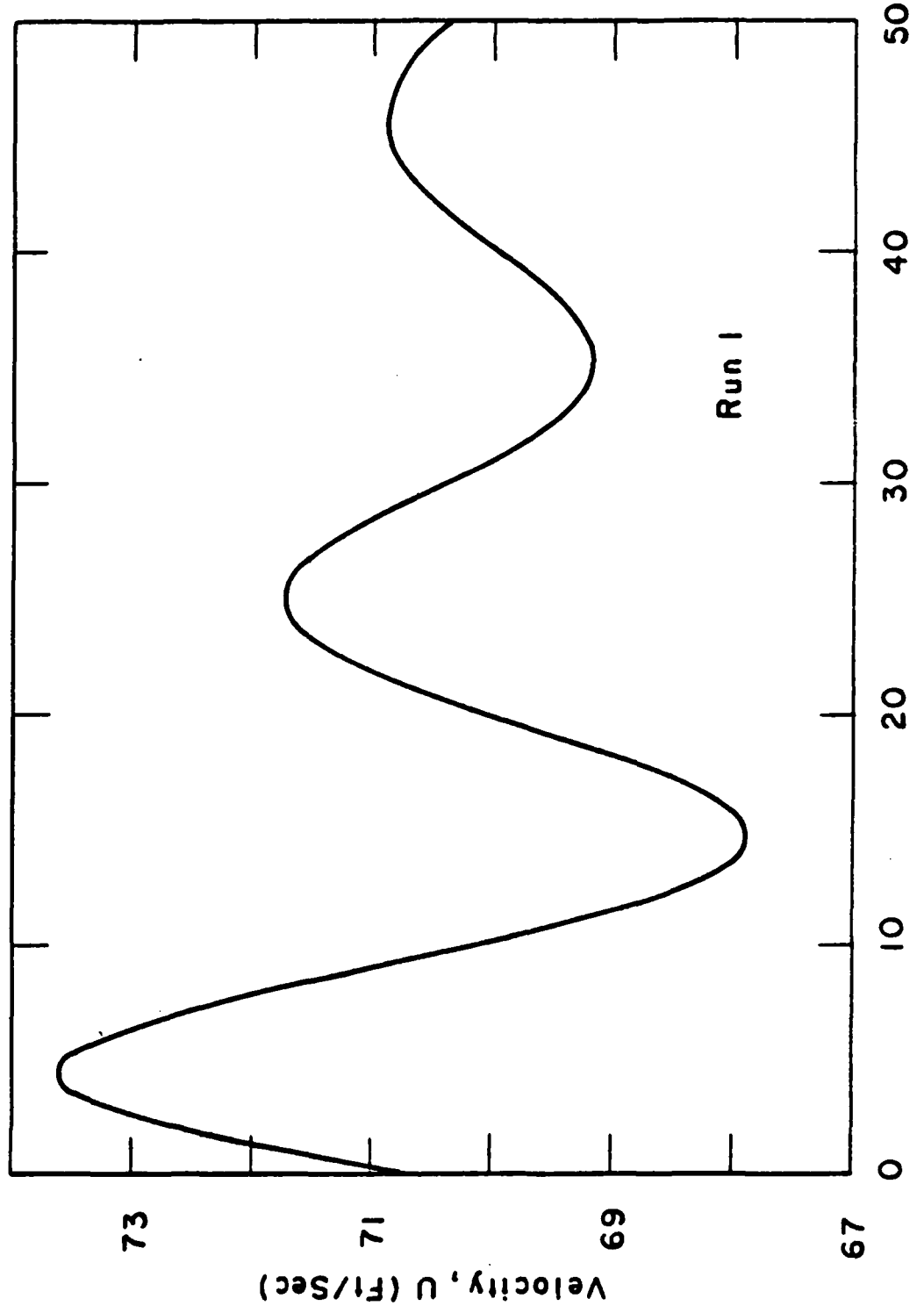

FIG. 7B PITCH PLANE SOLUTION FOR LONG TIME OR PHUGOID MOTION (LINEARIZED)

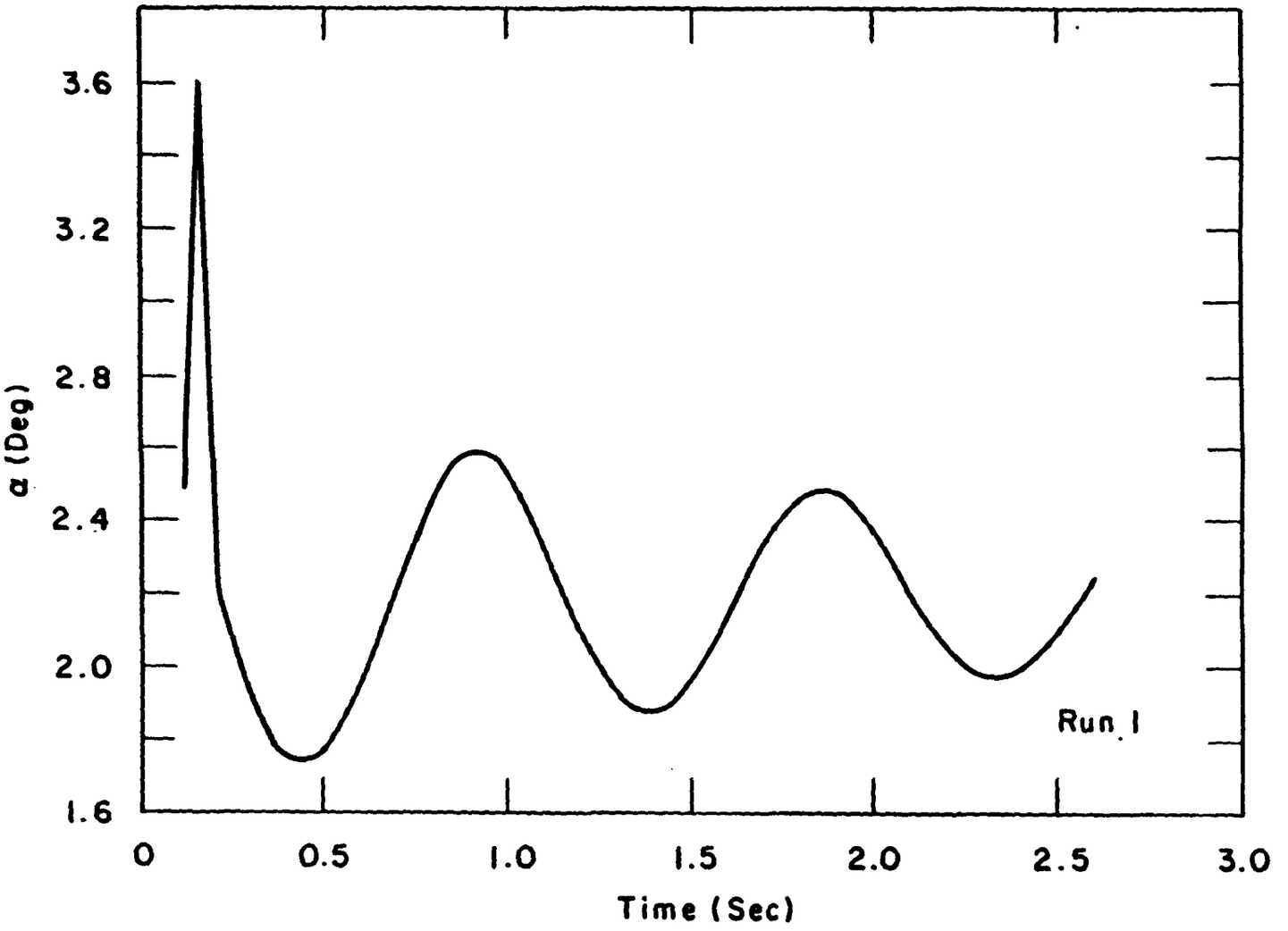

FIG. 8A NON-LINEAR MOTION $C_L = 2.33$, $\delta = 1°$ ANGLE OF ATTACK VARIATION

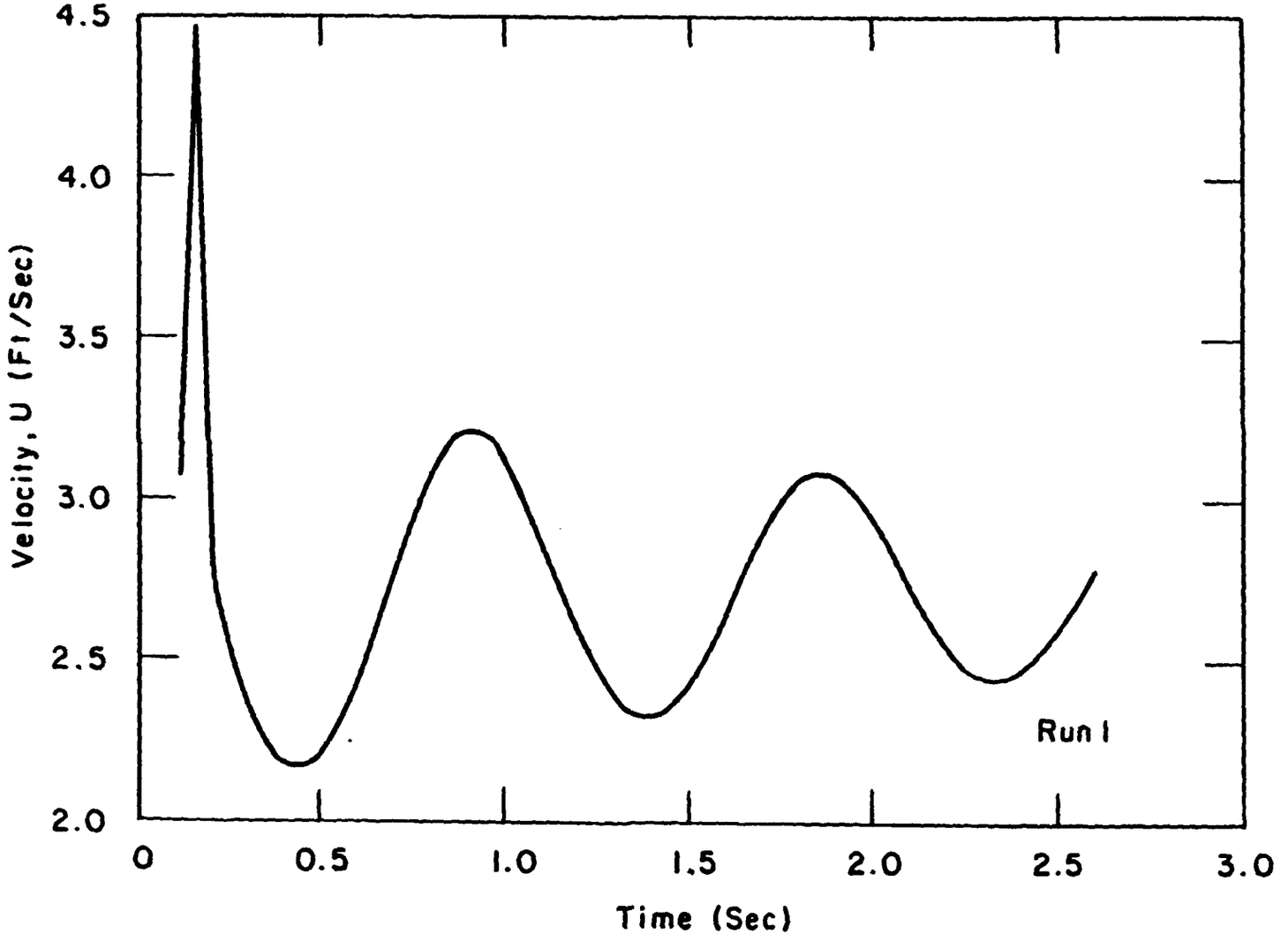

FIG. 8B NON-LINEAR MOTION $C_L = 2.33$, $\delta = 1°$ SHORT TIME VELOCITY VARIATION

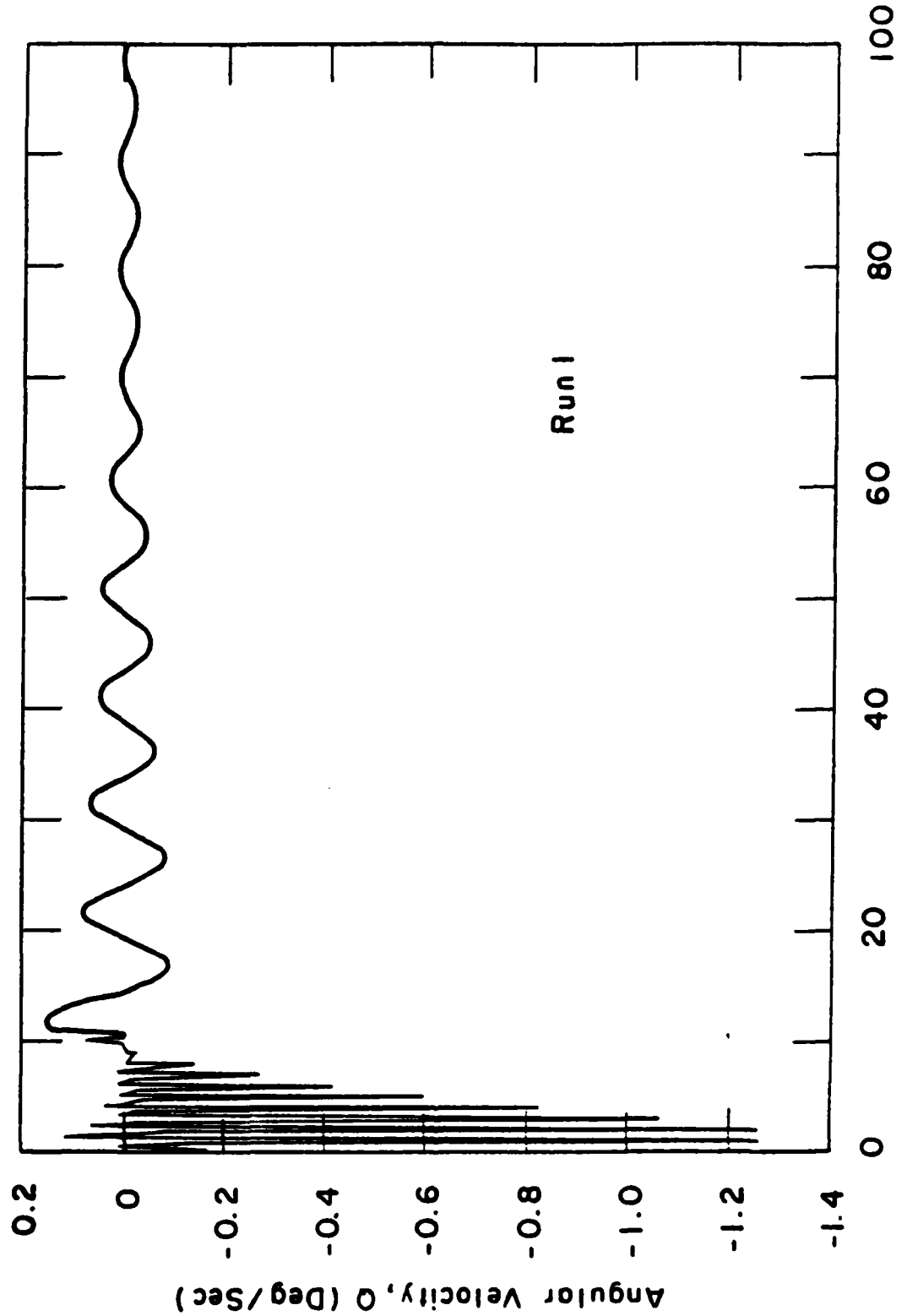

FIG. 8C NON-LINEAR MOTION $C_L = 2.33$, $\delta = 1°$ ANGULAR VELOCITY VARIATION

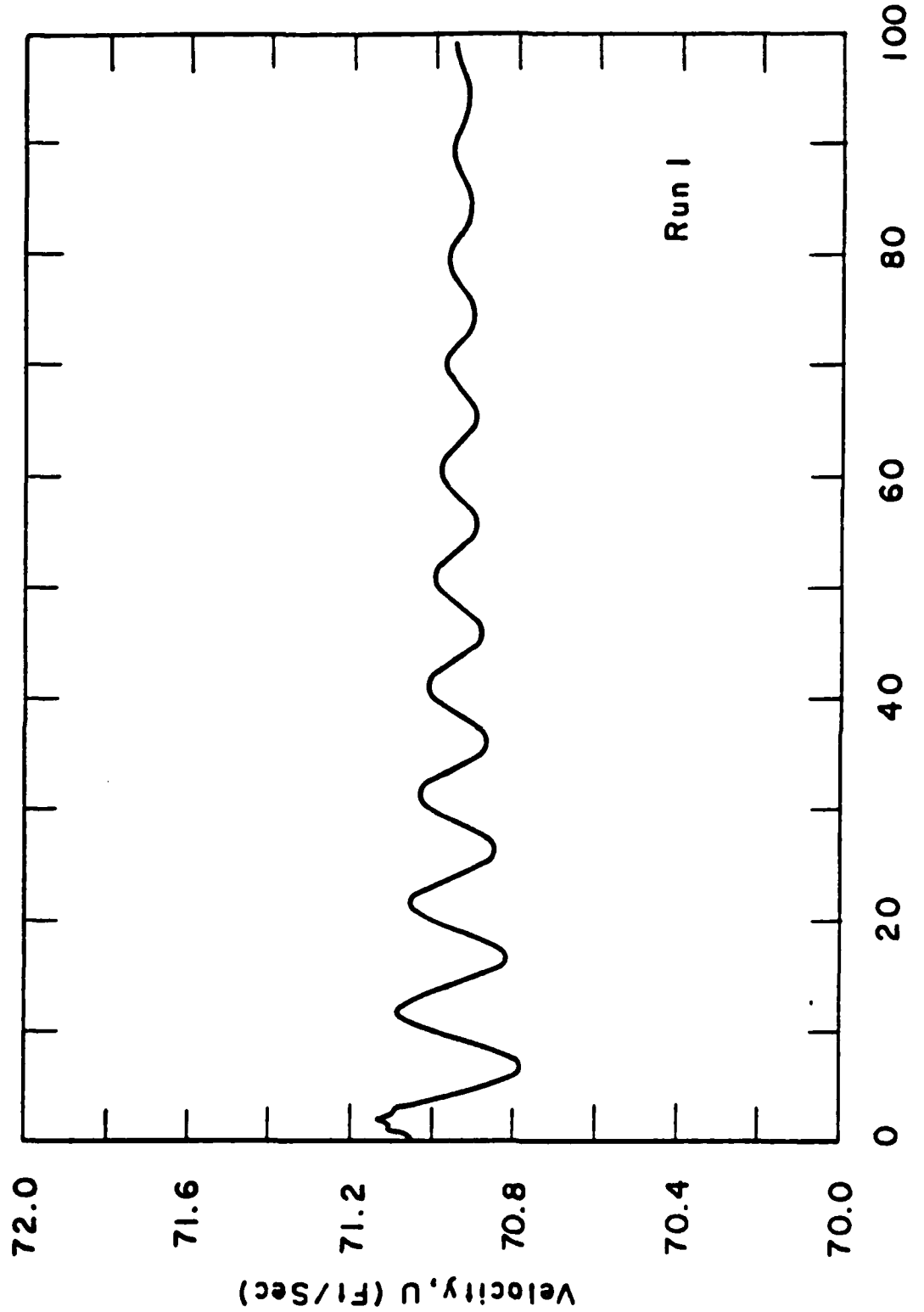

FIG. 8D NON-LINEAR MOTION $C_L = 2.33$, $\delta = 1°$ LONG TIME VELOCITY VARIATION

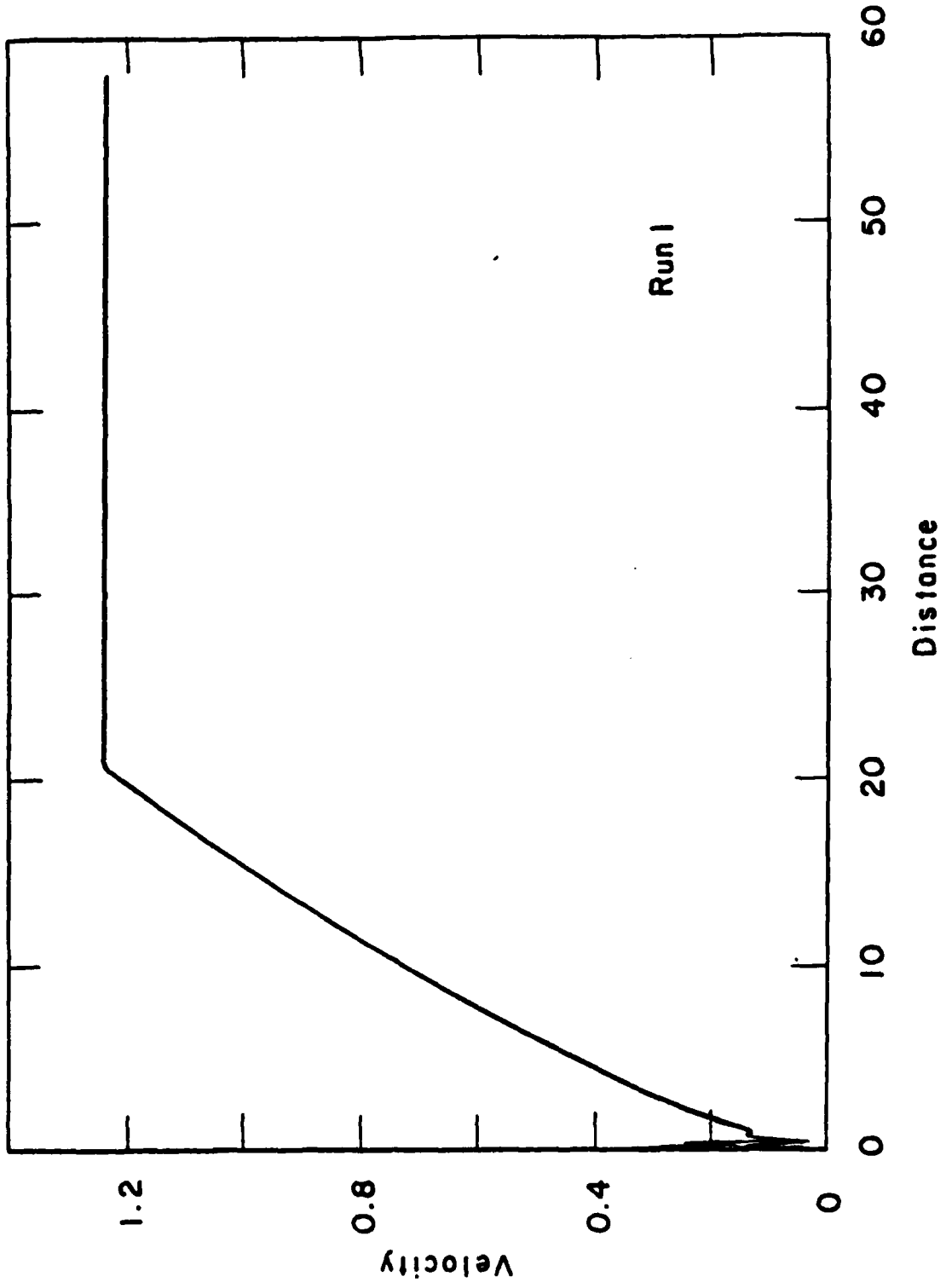

FIG. 9 LIAPUNOV STABILITY $C_L = 2.33$, $\delta = 1°$

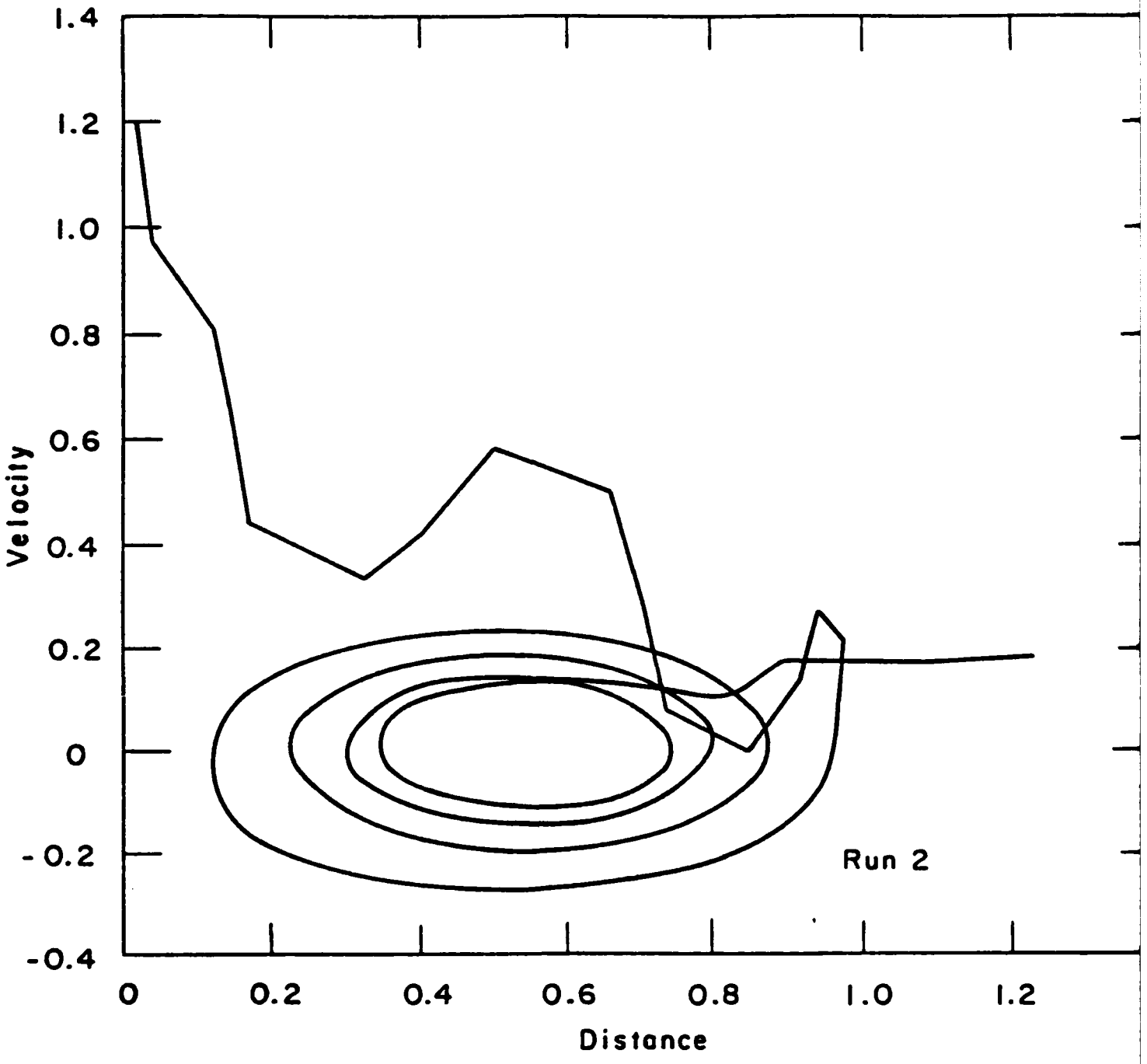

FIG. 10 LIAPUNOV STABILITY $C_L = 2.33$, $\delta = 2°$

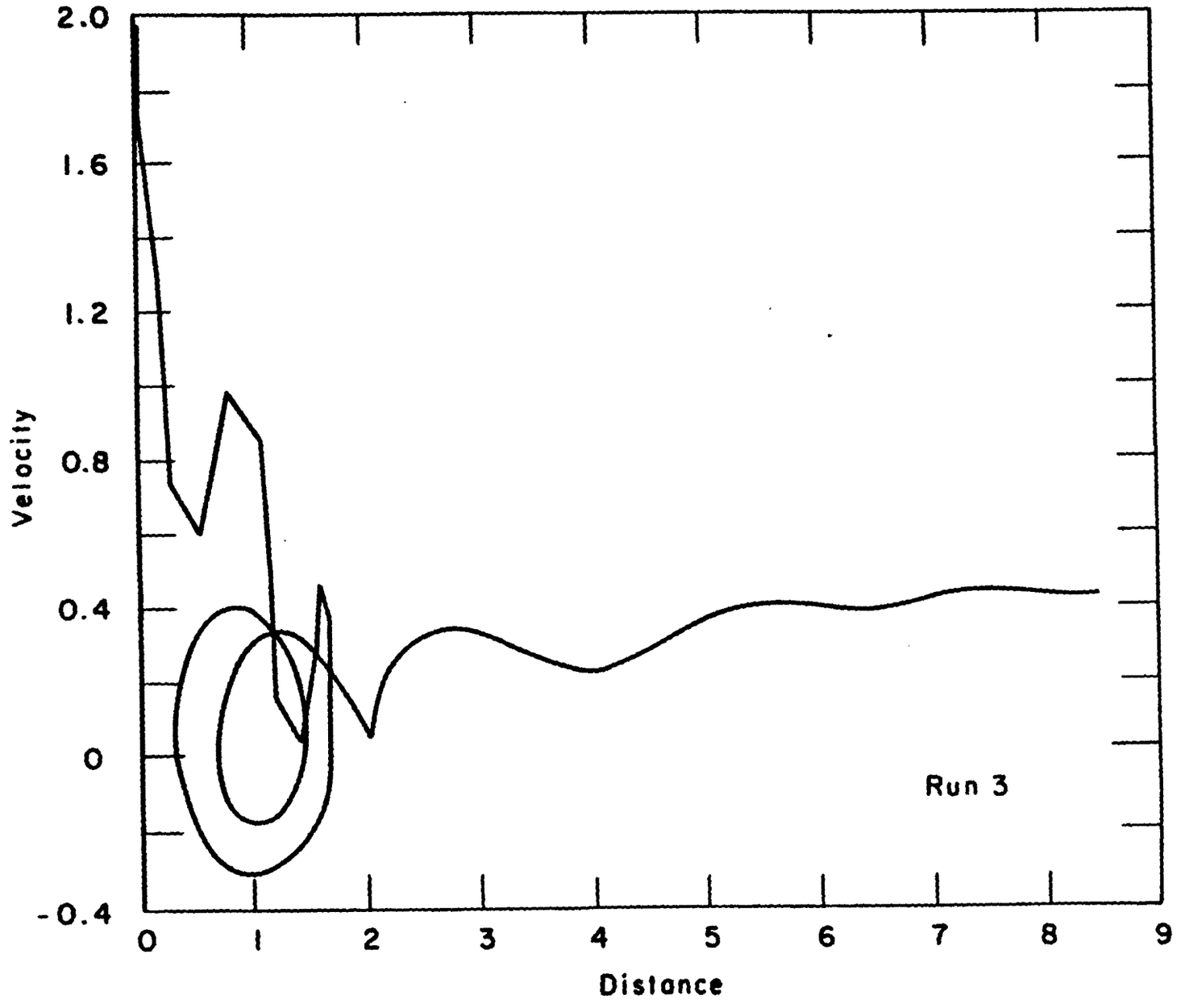

FIG. 11 LIAPUNOV STABILITY $C_L = 2.33$, $\delta = 4°$

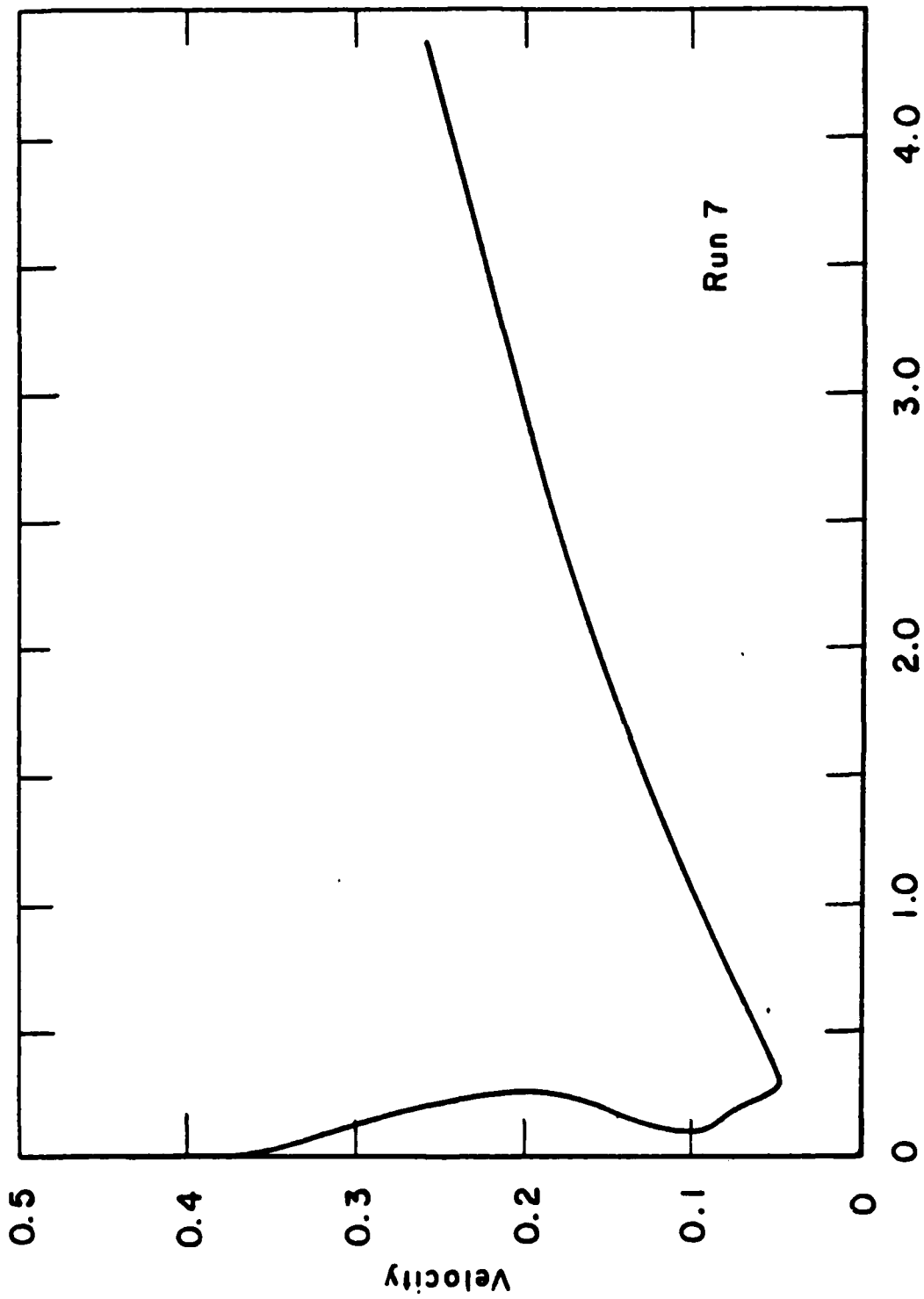

FIG. 12 LIAPUNOV STABILITY $C_L = 2.77$, $\delta = 1°$

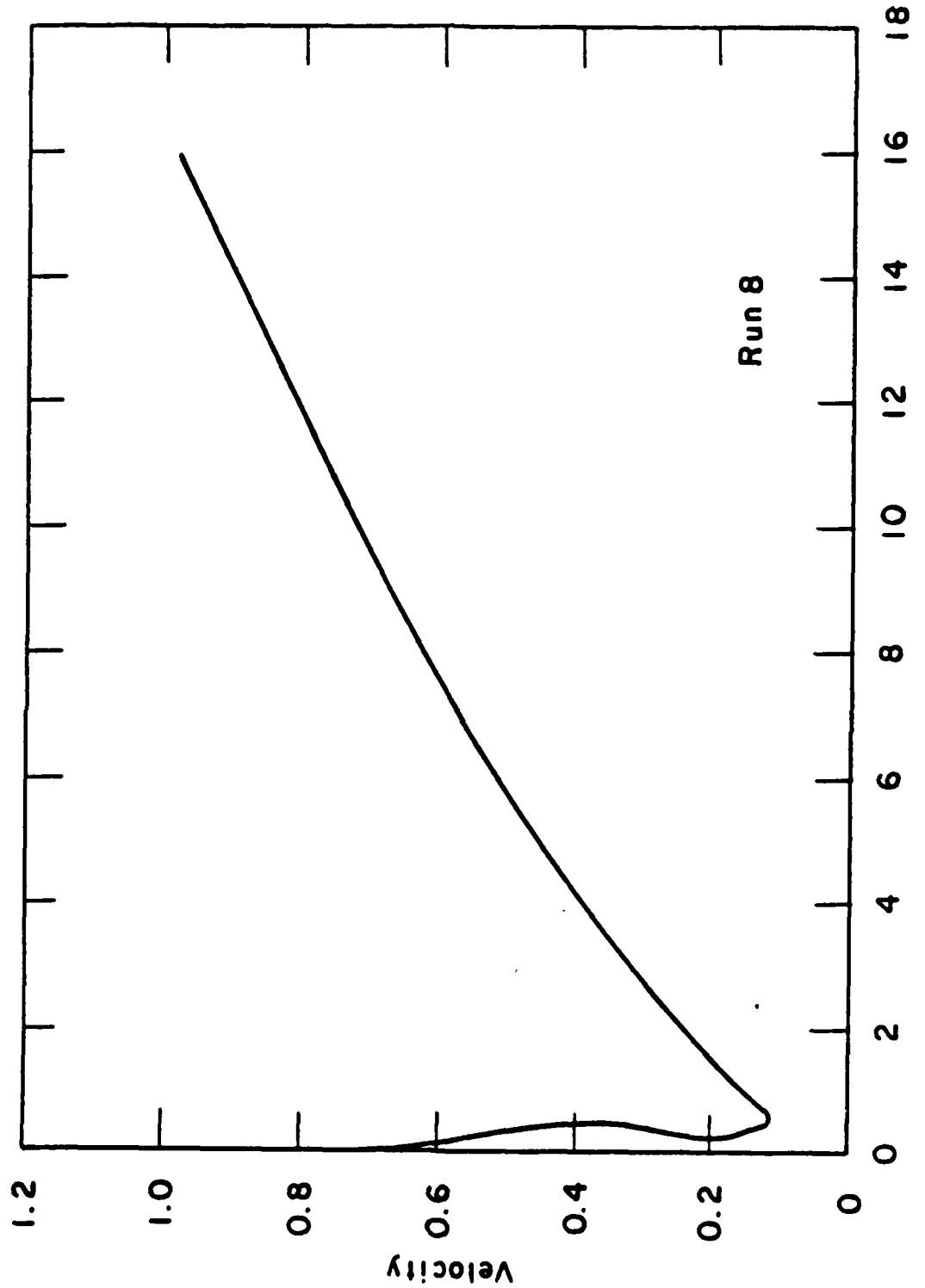

FIG. 13 LIAPUNOV STABILITY $C_L = 2.77$, $\delta = 2°$

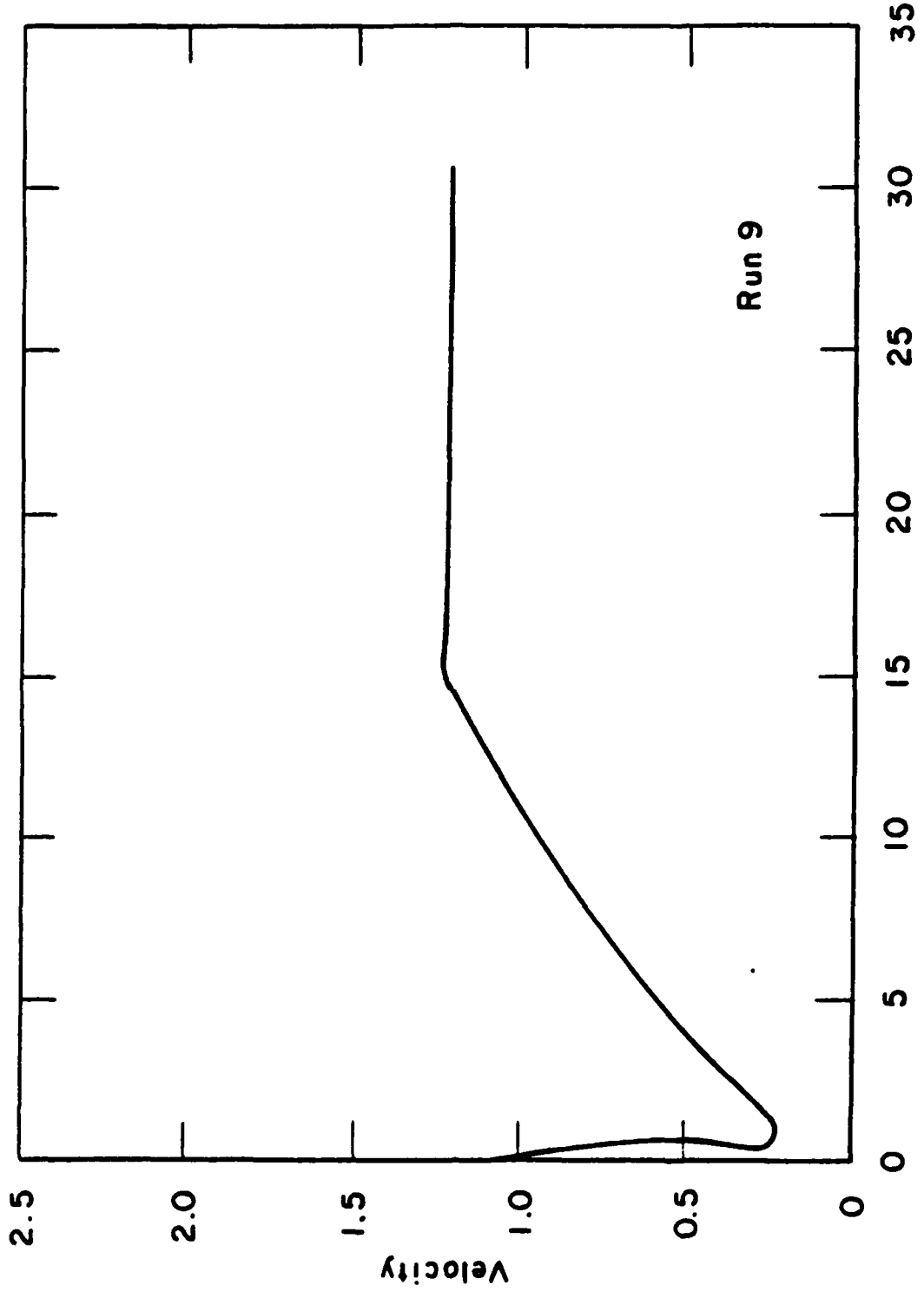

FIG. 14 LIAPUNOV STABILITY $C_L = 2.77$, $\delta = 4°$

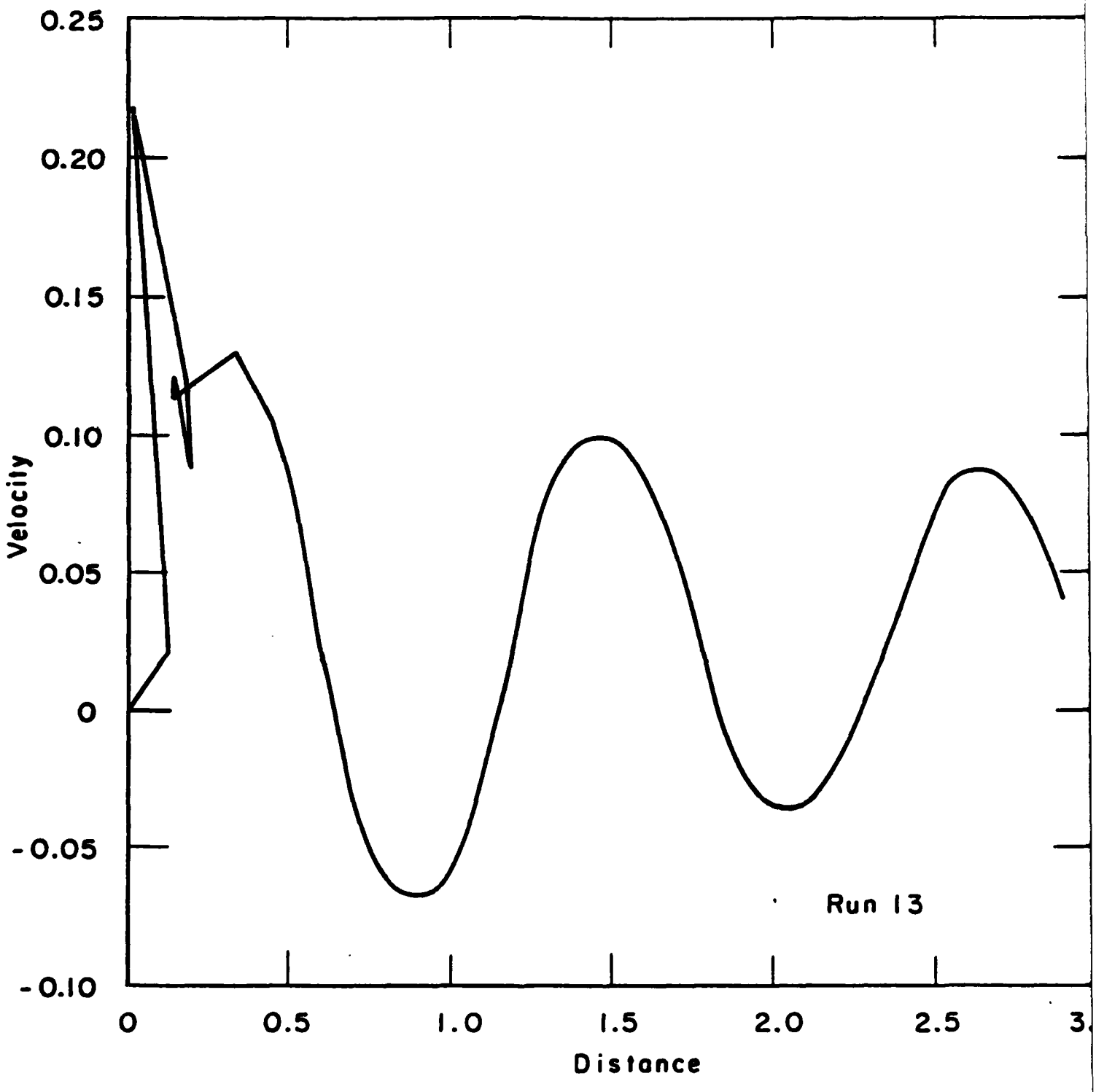

FIG. 15 LIAPUNOV STABILITY $C_L = 2.33$, $\delta = 0°$, YAW = 2°

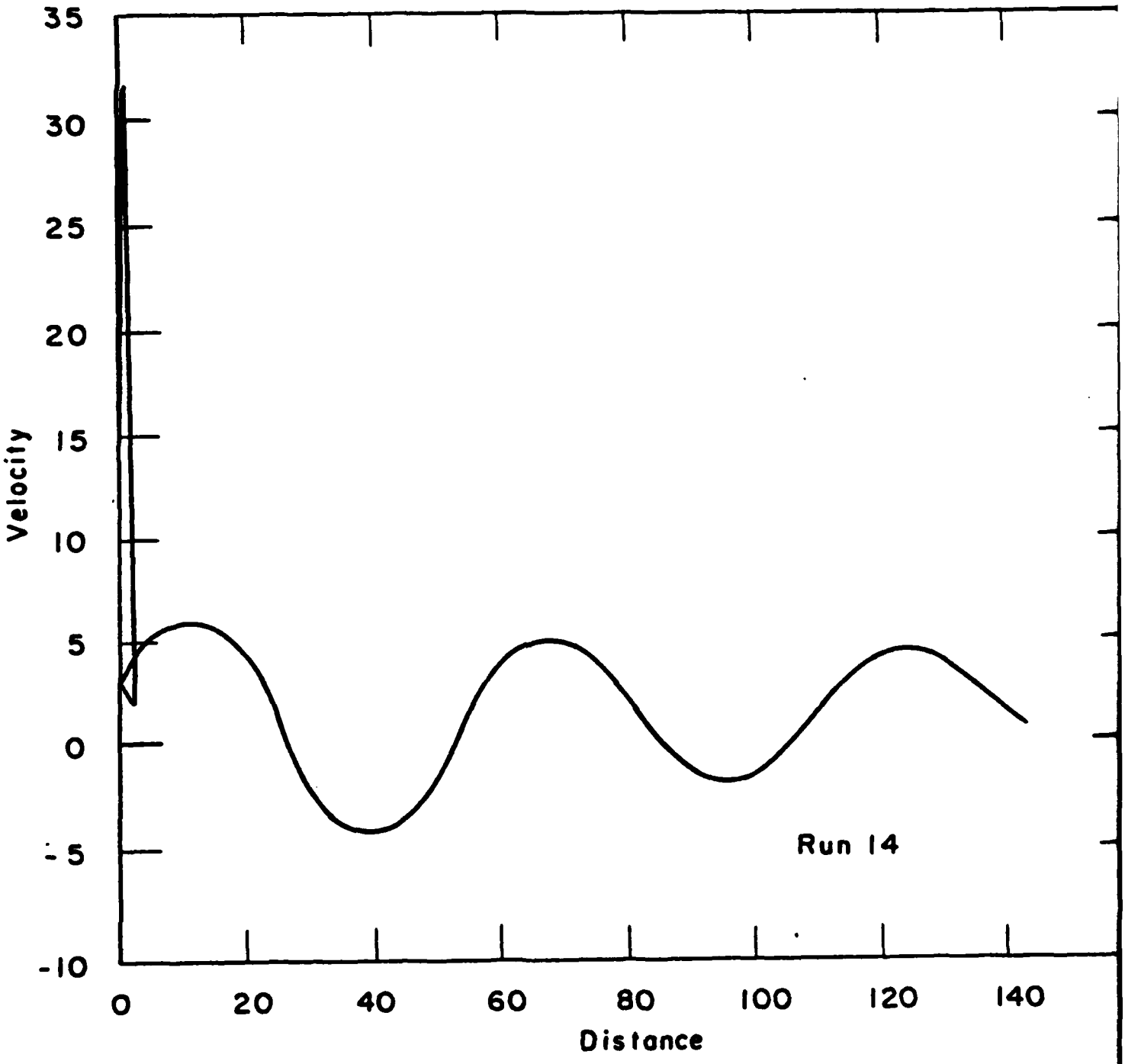

FIG. 16 LIAPUNOV STABILITY $C_L = 2.33$, $\delta = -1°$, LISSAMAN AIRFOIL

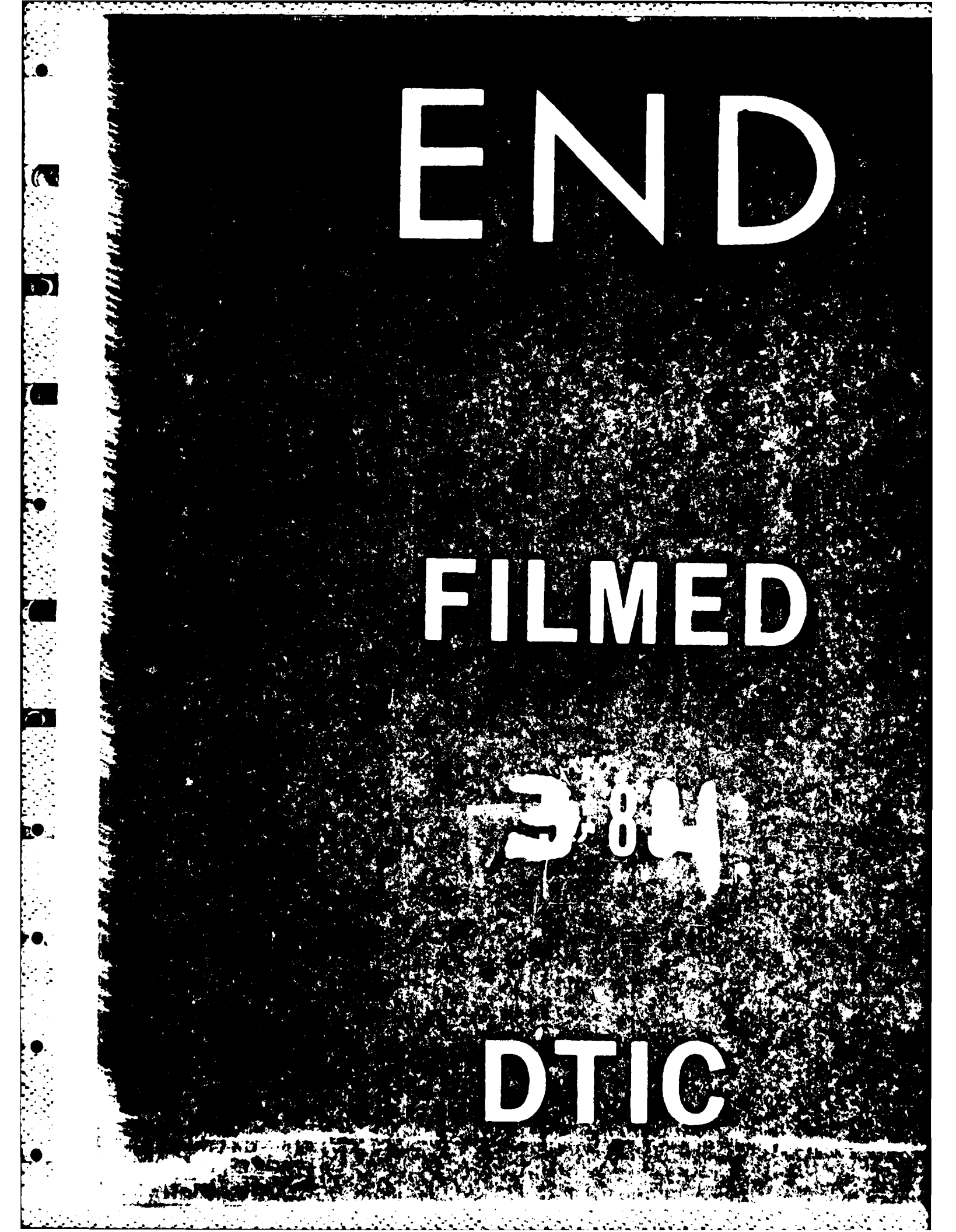
END
FILMED
3-84
DTIC